Universitat de Girona

Busigo Jean Jacques

Computational determination of knock down factors due to assembly tolerances in composite structures.

FRP++
Advanced structural analysis and design using composite materials

Master Dissertation
European Master Advanced Structural Analysis and Design using Composite Materials

Work developed under the supervision of
Professor Albert Turon Travesa
Professor José Manuel Guerrero García

Funded by the European Union

September 2025

DECLARATION

Name: Busigo Jean Jacques

Email: busigojj12@gmail.com **Phone number:** +34602404824

Citizen Card Number:

Title of the Dissertation: Computational determination of knock down factors due to assembly tolerances in composite structures.

Supervisors:

Professor Albert Turon Travesa

Professor José Manuel Guerrero García

Year of Conclusion: 2025

Master Course in Advanced Structural Analysis and Design using Composite Materials

University of Girona, 01/09/2025

Signature: 

ACKNOWLEDGEMENTS

I would like to begin by expressing my sincere gratitude to the MSc FRP++ board for granting me the opportunity to be part of this unique and prestigious program. Being selected for this master's has been a true privilege and a transformative experience in both my academic and personal journey. The program has opened doors to knowledge, cultures, and perspectives that I would not have encountered otherwise. It has been a journey filled not only with rigorous learning but also with invaluable adventures and experiences that will remain with me for a lifetime.

My deepest appreciation goes to all the institutions that make up this master's consortium. Each partner university has contributed in its own distinctive way to shaping my academic formation, broadening my vision, and nurturing my skills. The dedication of the professors, coordinators, and administrative staff has been crucial to the success of this journey, and I am sincerely grateful for their continuous support.

To my classmates, I owe a very special acknowledgment. Over the course of this master's, we became far more than colleagues; we became a family bound together by shared challenges, late-night study sessions, inspiring discussions, and countless memories across different countries and cultures. The friendships we have built are among the most valuable outcomes of this journey, and I will always treasure the laughter, encouragement, and solidarity we shared.

I also wish to express my heartfelt gratitude to my family. Their constant encouragement, prayers, and unconditional love have been my strongest source of motivation. Even in moments of doubt or difficulty, their words of support and belief in my abilities reminded me of the importance of perseverance and dedication. Without their foundation, this accomplishment would not have been possible.

A very special and sincere note of thanks goes to my supervisors, Professor Albert Turon Travesa and Professor José Manuel Guerrero García. I am very grateful to them for their guidance, patience, and unwavering commitment throughout the development of this thesis. Their expertise, critical insights, and constant availability were instrumental in shaping the quality of my work. I sincerely appreciate the time they invested in mentoring me, their encouragement in moments of uncertainty, and the knowledge they so generously shared. Working under their supervision has been an enriching experience from which I

have learned immensely, not only in the technical aspects of research, but also in both academic rigor, and scientific thinking.

Finally, I am grateful to all those who, in one way or another, have contributed to this journey. Whether through academic collaboration, a word of advice, or simple gestures of kindness, each contribution has played a role in bringing me to this milestone.

To all of you, I extend my deepest thanks.

Determinación computacional de factores de reducción debido a tolerancias de ensamblaje en estructuras compuestas

RESUMEN

Los materiales compuestos se utilizan cada vez más en aplicaciones estructurales de alto rendimiento debido a su superior relación resistencia-peso y a sus propiedades mecánicas adaptables a diferentes secuencias de apilado. Sin embargo, la variabilidad en la fabricación de agujeros y componentes introduce tolerancias geométricas que afectan a las tolerancias del ensamblaje. Estas tolerancias geométricas, a su vez, introducen tolerancias de ensamblaje, como desalineaciones entre agujeros o diferencias en el diámetro de los agujeros y la holgura entre los pernos, lo que afecta significativamente el comportamiento mecánico y la integridad estructural de las uniones compuestas. Como resultado, estas tolerancias inducen concentraciones de tensión alrededor de las superficies de apoyo debido a cambios en la dirección de la carga y, en última instancia, reducen el rendimiento general de la estructura. El objetivo principal de este estudio es modelar el efecto de las tolerancias de ensamblaje en el rendimiento estructural y evaluar los factores de derribo en uniones atornilladas de materiales compuestos aeronáuticos.

Este estudio desarrolla un enfoque de modelado integral estructurado en cuatro fases principales: en primer lugar, una estrategia de elementos finitos validada equilibra la precisión con la eficiencia computacional para una validación robusta del modelo. En segundo lugar, un código paramétrico de Python se utiliza para realizar estudios sistemáticos teniendo en cuenta variaciones de tolerancias. En tercer lugar, se genera un diseño de experimentos para la simulación de muestras atornilladas cuasi-isotrópas, incorporando incertidumbres clave como la desalineación entre agujeros y la holgura entre orificios y pernos, para cuantificar la variabilidad en el rendimiento estructural debido a los efectos de las tolerancias. Finalmente, se calculan los factores de derribo a partir del estudio de propagación de la incertidumbre para comprender cómo responde la estructura a las incertidumbres inducidas por el ensamblaje.

Los resultados proporcionan factores de derribo cuantitativos que permiten a los ingenieros considerar los efectos de la tolerancia en el diseño de uniones atornilladas compuestas, ofreciendo directrices cruciales para el cálculo del factor de seguridad y la predicción de la rotura. Esta investigación contribuye a un diseño de estructuras compuestas más fiable al establecer un marco sistemático para evaluar las incertidumbres inducidas por el ensamblaje en diferentes configuraciones de laminados.

PALABRAS CLAVE: Tolerancia de montaje; Desalineaciones de orificios, Valor B, Factor de derribo; Incertidumbres.

Determinació computacional de factors de reducció degut a toleràncies d'assemblatge en estructures compostes

RESUM

Els materials compostos s'utilitzen cada cop més en aplicacions estructurals d'alt rendiment a causa de la seva superio relació resistència-pes i les seves propietats mecàniques personalitzables a partir de diferents seqüències d'apilament. Tanmateix, la variabilitat de fabricació en la perforació de forats i la fabricació de components introdueix toleràncies geomètriques que afecten l'ajust del muntatge. Aquestes toleràncies geomètriques, al seu torn, introdueixen toleràncies de muntatge, com ara desalineacions entre forats i/o diferències en el diàmetre del forat i la folgança dels cargols, que afecten significativament el comportament mecànic i la integritat estructural de les unions compostes. Com a resultat, aquestes toleràncies indueixen concentracions d'esforços al voltant de les superfícies de suport a causa dels canvis en la direcció de la càrrega i, en última instància, redueixen el rendiment general de l'estructura. L'objectiu principal d'aquest estudi és modelar l'efecte de les toleràncies de muntatge sobre el rendiment estructural i avaluar els factors de reducció en les unions cargolades compostes aeronàutiques.

Aquest estudi desenvolupa un enfocament de modelització integral estructurat al voltant de quatre fases principals: en primer lloc, una estratègia d'elements finits validada equilibra la precisió amb l'eficiència computacional per a una validació robusta del model. En segon lloc, un códi paramètric de Python s'utilitza per estudiar sistemàticament la variació de tolerància de manera oportuna. En tercer lloc, es genera un disseny d'experiments per a la simulació de mostres cargolades quasi isotròpiques que incorpora incerteses clau com la desalineació forat a forat i la folgança forat-cargol, per quantificar la variabilitat en el rendiment estructural a causa dels efectes de les toleràncies. Finalment, es calculen els factors de reducció a partir de l'estudi de propagació de la incertesa per entendre com respon l'estructura a les incerteses induïdes pel muntatge.

Els resultats proporcionen factors quantitatius de reducció que permeten als enginyers tenir en compte els efectes de tolerància en el disseny d'unions cargolades de materials compostos, oferint pautes crítiques per als càlculs del factor de seguretat i les prediccions de rendiment. Aquesta investigació

contribueix a un disseny d'estructures compostes més fiable mitjançant l'establiment d'un marc sistemàtic per avaluar les incerteses induïdes pel muntatge en diferents configuracions de làmines.

PARAULES CLAU: Tolerància de muntatge; Desalineacions de forats, valor B, factor de deformació; Incerteses.

Computational determination of knock down factors due to assembly tolerances in composite structures.

ABSTRACT

Composite materials are increasingly being used in high performance structural applications due to their superior strength-to-weight ratios and customizable mechanical properties from different stacking sequences. However, manufacturing variability in hole drilling and component fabrication introduces geometric tolerances that affect assembly fit. These geometric tolerances in turn introduce assembly tolerances, such as hole to hole misalignments and/or differences in hole diameter and bolt clearance, which significantly affect the mechanical behavior and structural integrity of composite joints. As a result, these tolerances induce stress concentrations around bearing surfaces due to changes in the loading direction and, ultimately, reduce the overall performance of the structure. The main aim of this study is to model the effect of assembly tolerances on the structural performance and to assess the knock down factors in aeronautical composite bolted joints.

This study develops a comprehensive modeling approach structured around four primary phases: Firstly, a validated finite element strategy balances accuracy with computational efficiency for robust model validation. Secondly, a parametric Python framework enables systematic tolerance variation studies in a timely manner. Thirdly, a design of experiments is generated for the simulation of quasi-isotropic bolted specimens incorporating key uncertainties such as hole to hole misalignment and hole to bolt clearance, to quantify variability in structural performance due to tolerance effects. Finally, knock down factors are computed from the uncertainty propagation study to understand how the structure responds to assembly-induced uncertainties.

The results provide quantitative knock down factors that enable engineers to account for tolerance effects in composite bolted joint design, offering critical guidelines for safety factor calculations and performance predictions. This research contributes to more reliable composite structure design by establishing a systematic framework for evaluating assembly-induced uncertainties across different laminate configurations.

KEYWORDS: Assembly tolerance; Hole misalignments, B-value, Knock down factor; Uncertainties.

TABLE OF CONTENTS

CONTENTS

LIST OF FIGURES

LIST OF TABLES

LIST OF ABBREVIATIONS AND SYMBOLS

Abbreviations

CFRP	Carbon Fiber Reinforced Polymer
FEM	Finite Element Modelling
UQ&M	Uncertainty Quantification and Management
MS-PFA	Multi Scale Progressive Failure Analysis
FS	Factor of Safety
DLL	Design Limit Load
DUL	Design Ultimate Load
K/D	Knock down
KDF	Knock down Factor
DLJ	Double Lap Joint
GUI	Graphic user Interface
LG	Linear Geometry
NLG	Non-Linear Geometry
PDM	Progressive Damage Model
M&S	Modelling & Simulation

Symbols

E_{11}	Longitudinal Young's modulus of the CFRP ply
E_{22}	Transverse Young's modulus of the CFRP ply
G_{12},G_{13}	In-plane Shear's modulus of the CFRP ply
G_{23}	Out-of-plane Shear's modulus of the CFRP ply
ν_{12}, ν_{13}	In-plane Poisson's ratio for the CFRP ply
ν_{23}	Out-of-plane Poisson's ratio for the CFRP ply
E	Elastic modulus of the metallic parts
ν	Poisson's ratio of the metallic parts
X^t	Unidirectional longitudinal tensile strength
X^c	Unidirectional longitudinal compressive strength
Y^T	Unidirectional transverse tensile strength

Y^C	Unidirectional transverse compressive strength
G_{ft}	Longitudinal tensile fracture toughness
G_{fc}	Longitudinal compressive fracture toughness
G_{mt}	Transverse tensile fracture toughness
G_{mc}	Transverse compressive fracture toughness

1. CHAPTER ONE: INTRODUCTION

1.1. Motivation

Composite materials are increasingly being used in high-performance engineering applications, such as in aerospace, sports, wind energy, etc., due to their superior strength-to-weight ratios and design flexibility compared to traditional materials. In these applications, the performance of a structure is not only determined by the in-situ properties of the materials, but it also depends on the manufacturing quality and assembly accuracy. In mechanically fastened joints, structural integrity is influenced by assembly tolerances, especially bolt to hole clearances and hole misalignments. These geometric deviations often arise from the post-manufacturing processes (drilling, fitting, and misalignment during assembly) of the composite laminates, which can alter the load transfer between different components in the joint, leading to an unexpected response of the joint or even to a premature failure.

To design safe and reliable structures, engineers rely on design allowables for the material's strength, which are derived from the statistical analysis of experimental data [1]. These design allowables which can also be referred to as B-value, with a 95% lower confidence bound, simply mean that in a population made of n samples, at least 90% exceed the design allowable. These design allowables enables to determine the so-called “Knock down factor” (KDF) that accounts for different uncertainties in the material. However, current defined frameworks are only used to determine design allowables of the materials' strength of laminates. Therefore, it is crucial to isolate the effects of assembly-induced geometric uncertainties like bolt hole clearance and hole misalignments from other sources of variability, such as manufacturing variabilities.

With advances in computational modelling, it has become possible to quantify these effects using high or low fidelity finite element simulations that incorporate geometric deviations. Through these approaches, uncertainties arising from assembly tolerances can be systematically explored without extensive experimental campaigns. By propagating the uncertainties, it is possible to simulate the effect of hole misalignments and bolt hole clearance on the joint stiffness, first knee point load and first load drop. After, by statistically processing the results following the composite materials military handbook (CHM-17) [2], the knock down factors can be determined and directly attributed to these uncertainties.

This study aims to computationally determine knockdown factors arising from assembly tolerances—specifically bolt-hole clearances and hole misalignments—in composite structures. The methodology employs finite element modelling to simulate tolerance effects, followed by statistical analysis to estimate B-values from the simulation data. By quantifying how assembly tolerances affect structural performance, this research bridges the gap between manufacturing reality and structural design, enabling more accurate tolerance management in composite assemblies.

1.2. Objectives

The main objective of the study is to model the effect of manufacturing assembly tolerances on the structural performance of composite bolted joints to determine the KDF. To achieve this objective the following specific objectives need to be completed:

- Define the Modelling and Simulation (M&S) strategy for a bolted joint configuration.
- Generate parametrized FE models of joints with the presence of assembly tolerances.
- Elaborate a methodology to propagate the uncertainty associated with the presence of assembly tolerances in the structure.
- Quantify the uncertainty associated with the presence of assembly tolerances.
- Obtain the knock down factors on the composite structure as a function of the laminate configuration (QI, hard, soft).

1.3. Structure of the dissertation

This dissertation is organized in five chapters, namely: Introduction, Literature review, Methodology, Case study, Results and discussion, and Conclusions. Chapter 1 briefly talks about the motivation, main objectives, and specific objectives of the study. Chapter 2 presents a literature review focusing on the effects of different fittings and hole misalignments, computational techniques used, how design allowables are applied to mean static strengths of a structure, and the existing gaps in the literature. Chapter 3 describes how the objectives will be achieved by defining the modeling and simulation approach for a bolted lap joint, detailing how a parametric Python script can be developed for the model generation, elaborating on the method for uncertainty propagation, using the CMH-17 approach for UQ&M, and finally, how the knock down factors can be obtained. Chapter 4 applies the defined methodology in Chapter 3 to

a case study with a single lap double bolt joint configuration. The B-values for three quantities of interest, and the knock down factors due to uncertainties that were propagated in the structure are computed and analyzed. Finally, Chapter 5 closes the study, detailing the practical implications of the findings, limitations, and future work.

2. CHAPTER 2: LITERATURE REVIEW

2.1. Introduction

Composite materials are widely employed in high-performance structural applications, such as in aerospace, due to their high strength-to-weight ratio and customizable mechanical properties that can be achieved through different ply stacking sequences. Most composite components are made of unidirectional prepreg tapes and they are being applied in fields where joints are necessary [3]. Three types of joints are commonly used in composite structures, namely, mechanically fastened joints, adhesively bonded joints, and hybrid joints [3]. In mechanical fastened joints, bolted joints are the mainly used joining techniques due to the advantages they offer, such as high load bearing capacity and ease of assembly and disassembly [3, 4]. However composite laminates are not manufactured with holes, hence there is a need for manufacturing the holes by drilling [5, 6, 7]. Hole fabrication processes introduce geometric variations that generate different fit tolerances, i.e., clearance fit (Figure 2.1).

The stress distribution in a bolted joint is affected by different parameters, namely the stacking sequence, bolt to hole clearance, bolt preload [8], and hole misalignments. To design a safe and reliable bolted joint, it is essential to understand the effect of each parameter as it affects the structural performance differently. Each of the above parameters, once changed from what is considered the nominal configuration of the joint, can be interpreted as an uncertainty. Each uncertainty introduces a knock down factor in the structure that, in return, alters the overall performance of the structure.

2.2. Assembly tolerances

Assembly tolerances are crucial in manufacturing engineering as they define allowable differences in terms of the geometry and positioning of the part to ensure proper fit and functionality of assembled structures. In applications that require high precision while keeping the structures cost efficient, deciding on what tolerances to be used becomes very important since they impact both quality and cost of manufacturing [9]. Hence, there is a need to understand the tolerances during manufacturing and assembly. Tolerances can be classified according to different interactions between parts and the changes

that they introduce in the structure. Different geometric tolerances introduce assembly tolerances in a structure, i.e., bolt hole clearance and hole misalignments [9].

Bolt to hole clearance is a critical parameter in the design of composite joints, as even slight changes in its dimensions can significantly alter load transfer and the initial stiffness, thereby affecting the joint's overall performance. By adjusting the dimensions of the bolt to hole clearances, two types of fittings are possible: clearance fit and interference fit.

On the one hand, clearance fit is a bolted joint configuration where there is a gap between the bolt and the hole, allowing the bolt to rotate freely. Numerical and Experimental studies show the effect of clearance on the joint's stiffness, strength, load distribution, and fatigue life. An increase in clearance reduces the joint stiffness, which is due to a reduction in the area of contact between the bolt shank and the bearing surface [10, 11], as it can be seen in Figure 2.1. Kelly et al. [11] investigated the effect of clearance on bearing strength of a joint and established that at 4% hole deformation of the composite laminate, there was a decrease of 7% and 19% in bearing strength for the bolt-hole clearance levels of 1.55% and 3.05%, respectively [11]. McCarthy et al. [10] studied the effect of bolt hole clearance on joint stiffness for nominal clearance values of 0, 80, 160, and 240 μm, and observed a decrease in joint stiffness as the clearance increased, reaching a reduction of 10-11% at 240 μm [10]. Lawlor V et al. [12] investigated the effect of clearance on initial failure and load distribution in multi-bolt joints. It was found that the initial primary failure occurred at a much lower load for joints with clearance compared to net fit joints. With different values of clearances in different bolts, there was a change in the load distribution, which was observed in bolts with high clearances carrying little to no load initially causing uneven load distribution [12].

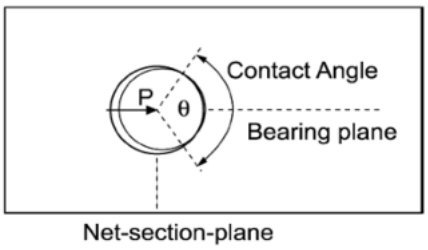

Figure 2.1: Contact angle for bolt-hole bearing with a clearance [11].

On the other hand, interference fit is a joint configuration where the bolt shank diameter is slightly larger than the hole diameter, and it can also be referred to as a force fit. Contrary to a clearance fit, interference fits offer better joint performance by increasing the load bearing capacity, through an increased surface

contact between the bolt and the hole. This is achieved by a local pre compression stress that is introduced around the hole surface, which in return reduces the magnitude of tensile stresses under mechanical loading [8, 13]. In interference fit there is also a reduction of stress concentration around the contact surface, which is achieved through a delay in the bolt inclination that inhibits the stress concentrations; this is beneficial to joints that are susceptible to net-tension failure and shear-out failure [4, 8]. Although the use of interference fit shows great benefits, during installation of the bolt damages that can be introduced in the composite such as delamination, matrix cracking and fiber failure resulting in an overall detriment of the joint performance [14]. Thus, it is crucial to use the appropriate interference fit size to achieve desirable outcomes. In this regard, Cao Y et al. [13] reported that peak joint performance can be achieved with 0.5% interference size, beyond which there is a decline in the performance caused by the installation damage.

Further to this, hole misalignment is another important assembly tolerance, and it has a significant effect on the composite structure as do the different fittings. It can manifest as a hole perpendicularity error, which can be defined as the degree to which the drilled hole deviates from the bolt longitudinal axis, leading to the formation of tilted holes, see Figure 2.2.

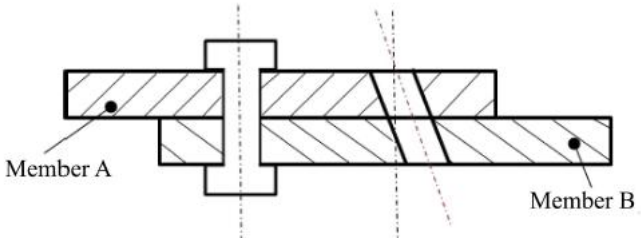

Figure 2.2 Hole perpendicularity [15].

Hole perpendicularity has a significant effect on the load distribution in a multi-bolt joint configuration and this leads to an introduction of residual forces in the structure (Figure 2.3). The load distribution in multi-bolt composites is altered due to the presence of residual forces that arise from uneven assemblies due to the bolts that are installed in a tilted position [15].

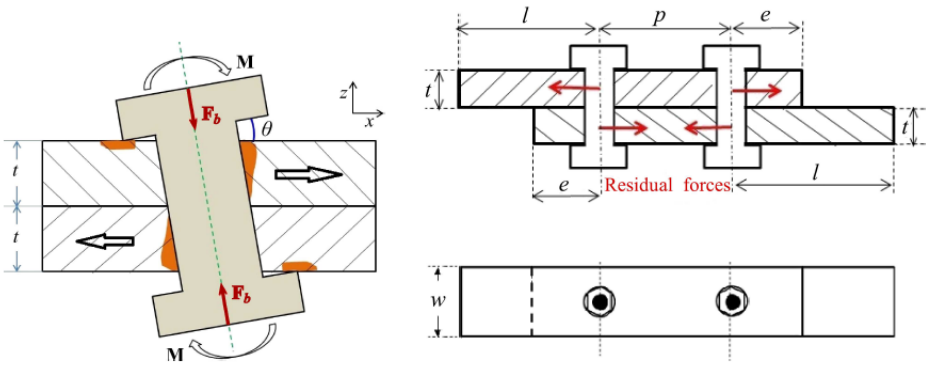

Figure 2.3: Residual stresses arising from hole perpendicularity error [15].

Hole tilting angle is a crucial parameter as suggested by Li et. [15], if the holes happen to be tilted in the opposite direction from the loading direction, one of the components making the joint will bear 60% of the load.

2.3. Computational Methods

Robust computational methods are essential in order to analyze and understand the behavior of composite joints, while also providing an insight on potential failure modes, stress concentrations and load distributions.

2.3.1. Finite Element Modeling

Thanks to the advancements in the designing of composite materials and computational resources, finite element modelling (high fidelity and low fidelity) is slowly replacing or complementing the analysis that used to be carried out through extensive experimental campaigns [16]. When performing uncertainty analysis, which require a relatively large design of experiments, it is mandatory to choose the level of model fidelity depending on computational resources available.

Low fidelity finite elements models are computational efficient, easy to implement since they do not need advanced material characterization, but they are less accurate due to their inability to capture complex phenomenon observed in composite materials [17]. On the contrary, high fidelity models are more accurate, but require more computational resources and advanced material characterization [17] that is not directly available at commercial finite element programs and must be implemented using advanced user subroutines. In applications where safety is a must, high-fidelity models are preferred in the validation

process while low fidelity models can be used during the preliminary design process because of the needed large number of iterations made in the designs [18, 19].

These approaches can be implemented through commercial finite element programs like ABAQUS/CAE, ANSYS or LS-DYNA, and can be used to model the damage initiation, damage evolution, predicting the stiffness, strength and deformation of a composite structure. Finally, it can be employed to visualize delamination and crack propagation by the use of cohesive zone models. In the existing literature different authors use high fidelity finite element modeling validated by experimental campaigns to examine different aspects of composite structures or composite laminates. G. Kolks et al. [20] developed a progressive damage model aimed to predict the mechanical behavior of CFRP bolted joint under tensile loading. The model utilizes energy degradation strategies and damage activation functions based on LaRCO3 and LaRCO4 failure criteria. Ca0 Y et al. [13] used a progressive damage model based on improved 3D Hashin criteria to investigate the effects of clearance and interference sizes in composite structures. The findings from the simulations were validated by experimental results with an error percentage of less than 5% [13]. With FEM it is also possible to analyze stress concentrations and load distributions in a structure as reported in [11, 15].

2.4. Determination of B-value using simulations

B-values are design allowables for material strength that are statistically based, and they take into account variabilities of manufacturing process, geometry and material properties [21]. These design values are used in aeronautics to properly size critical components of the structure [22]. From the CMH-17 [2] definition, the B-value is the 95% lower confidence bound where the 90% of the values of material strength is expected to exceed the B-value computed [2, 21, 22]. To determine the B-value, a large number of samples are needed to account for all the variabilities, e.g., due to manufacturing processes, geometry, properties, loading conditions and even the environment where the composite is being used. As a result, it is time consuming and costly to determine design allowables through experimental testing only [21, 22]. G. Abumeri et al [22] proposed an approach to determine design allowables with reduced testing which can be achieved through material property characterization at lamina level testing, the use of MS-PFA in combination with probability distribution to produce a scatter function as obtained from testing [22]. Alternatively, the B-value can be obtained through numerical simulations, e.g. [21, 23] as it will be done in this work as well.

2.5. Knock down factor determination and application on a structure

A knock down factor is a strength reduction factor that is applied to the structural or material strength to account for uncertainties in the material composition, geometry, and environmental application [24]. In composite materials, a knock down factor can be determined with a focus on only one source of uncertainty or a combination of several uncertainties, the later providing a more reliable structural design. Ninyerola et al [23]. Proposed a validated simulation methodology to obtain design allowables by both deterministic validation and non-deterministic validation and obtained the knock down factors on a single lap shear strength [23].There are four approaches proposed by Van Wagenen [24] to apply the knock down factors on structures under static loading conditions.

In the first approach all the uncertainties (materials, environment, structural) are combined under a single factor of safety and no knock down factor is used. Hence, this leads to the use of a large safety factor (see Figure 2.4), leading to a conservative design. This approach is only applicable to cases where there is high uncertainty on material properties [24].

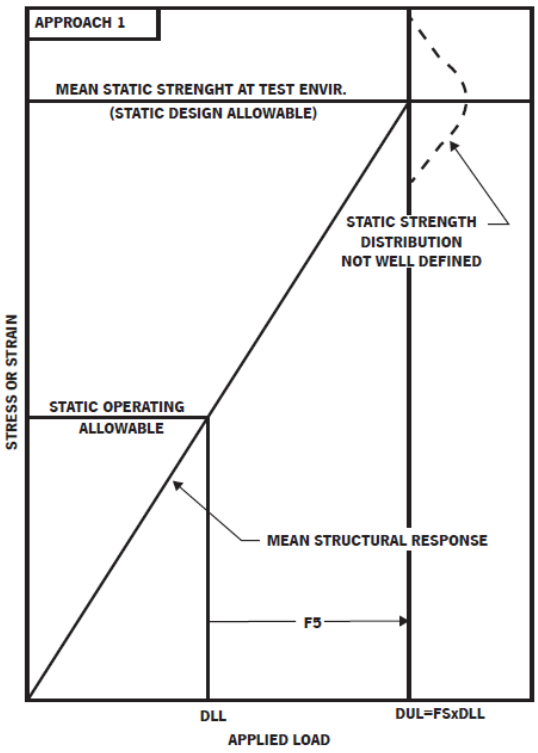

Figure 2.4: Approach 1, with all uncertainties combined in a single factor of safety [24].

In the second approach (Figure 2.5), the safety factor is only used to account for uncertainties with limited known effect and knock down factors that account for environmental and strength variabilities that are obtained from testing [24].

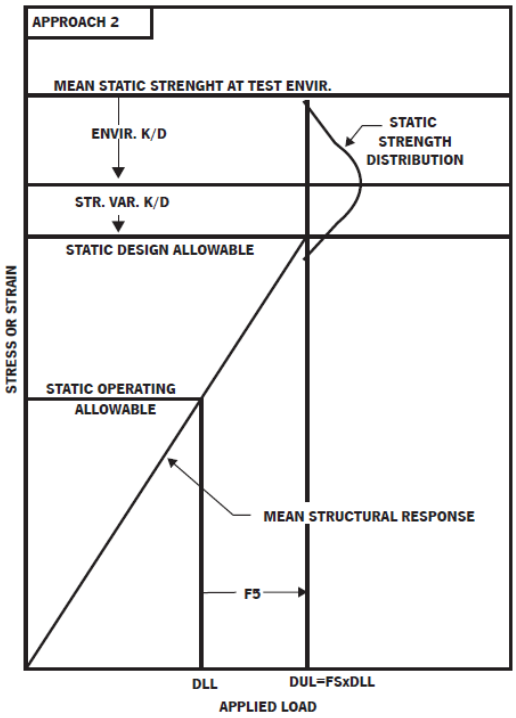

Figure 2.5: Approach 2, accounting for well-known effects from uncertainties due to environment and strength variability [24].

Alternatively, approach 3 (Figure 2.6) includes the structure response variability on top of the structure factors in the mean knock down factor instead of a factor of safety. With this method additional uncertainties can be removed but due to the need of using strain gauges, the results might have errors due to the influence of the environment [24].

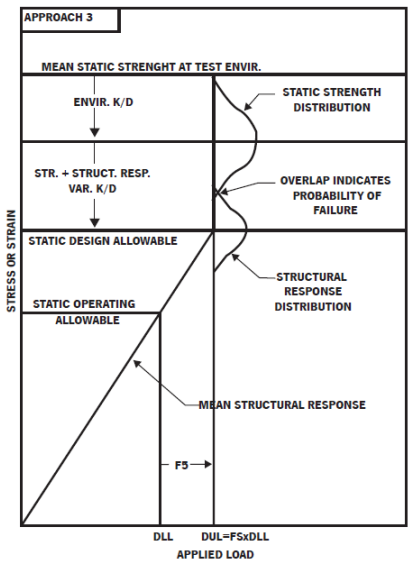

Figure 2.6: Approach 3, structural response variability combined with the effect of strength variability in a single knockdown factor [24].

Finally, approach 4 (Figure 2.7), considers a less standard approach to account for all uncertainties. Sufficient knock down factors are applied to the mean static strength and to introduce additional conservatism in the design, a factor of safety is applied from 1.0 to 1.5 [24].

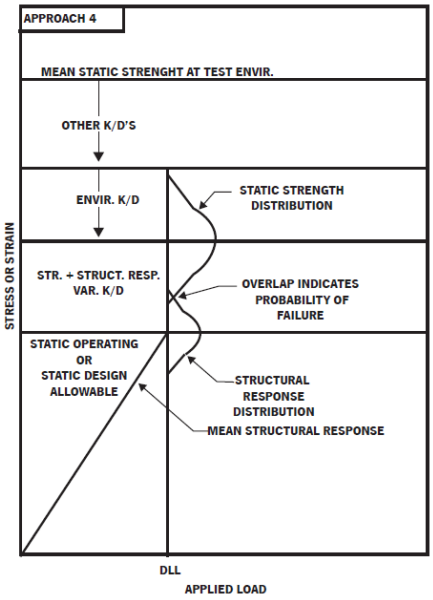

Figure 2.7: Approach 4, knock down factors applied to the static mean strength [24].

2.6. Research gaps and conclusion

There have been some studies on the effects assembly tolerances have on composite structures, either in double lap joints or single lap joints with single or multiple bolts. Still, there is no defined framework for determining knock down factors on composite bolted joint structures due to tolerances.

Current literature used a deterministic approach to quantify and analyse the effect of some parameters, such as the bolt hole clearance, highlighting their impact on the structure's performance [4, 10, 12, 13]. However, in real-world structures, the uncertainties present are fully randomized and not consistent from structure to structure, and each level of bolt hole clearance present in the structure introduces hole misalignments. Hence, a step forward is needed in the literature.

Moreover, methods that are available to determine the design allowables do not isolate the effects of assembly-induced geometric uncertainties [21]. Due to that, there is limited knowledge on how much these tolerances affect the structure's design allowable while accounting for different uncertainties, i.e.

hole clearances, hole misalignments and different material stacking sequences, since changing any of these will alter the overall structure behavior.

3. CHAPTER 3 METHODOLOGY

3.1. Introduction

This chapter presents the methodology of how to model all the uncertainty tolerance parameters for the composite bolted joint case that will be analysed in this work see Figure 3.1. This will be done by defining the modelling and simulation strategy, generating a parametric Python script for preparing the case study (a composite bolted joint with 2 bolts), uncertaintity quantification for design of experiment to introduce reasonable variations in the structure, UQ&M to ensure the variations and risks are correctly addressed, and finally, compute the knock down factors due to the assembly tolerances to provide an insight on structure performance.

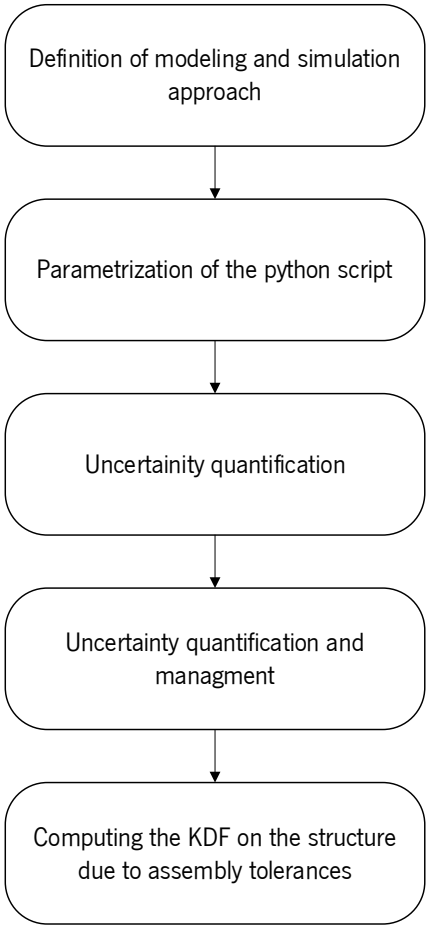

Figure 3.1: Workflow from definition of modeling and simulation approach to KDF computation highlighting necessary steps undertaken.

3.2. Definition of modelling and simulation approach

Different strategies can be used to model a structure's behaviour, but for this study, finite element modelling using the ABAQUS commercial program was chosen. This was done to develop and validate a robust model to be used to predict the behaviour of the structure with accuracy, but also while keeping in mind computational time and costs. The bolted joint case study that will be investigated in this work is a composite – composite single lap joint with 2 bolts, as it will be shown in Chapter 4. However, since a 2 bolted joint is very complex, this work started with a simpler model with 1 bolt. Therefore, to ease the explanation of the simulation strategy, this chapter will present all the methodology with the case of a bolted joint with a single bolt, which will be referred to as a double lap specimen. Figure 3.2. presents this simpler specimen with two metallic arms made of titanium, a titanium bolt, and a composite laminate (T800 carbon epoxy).

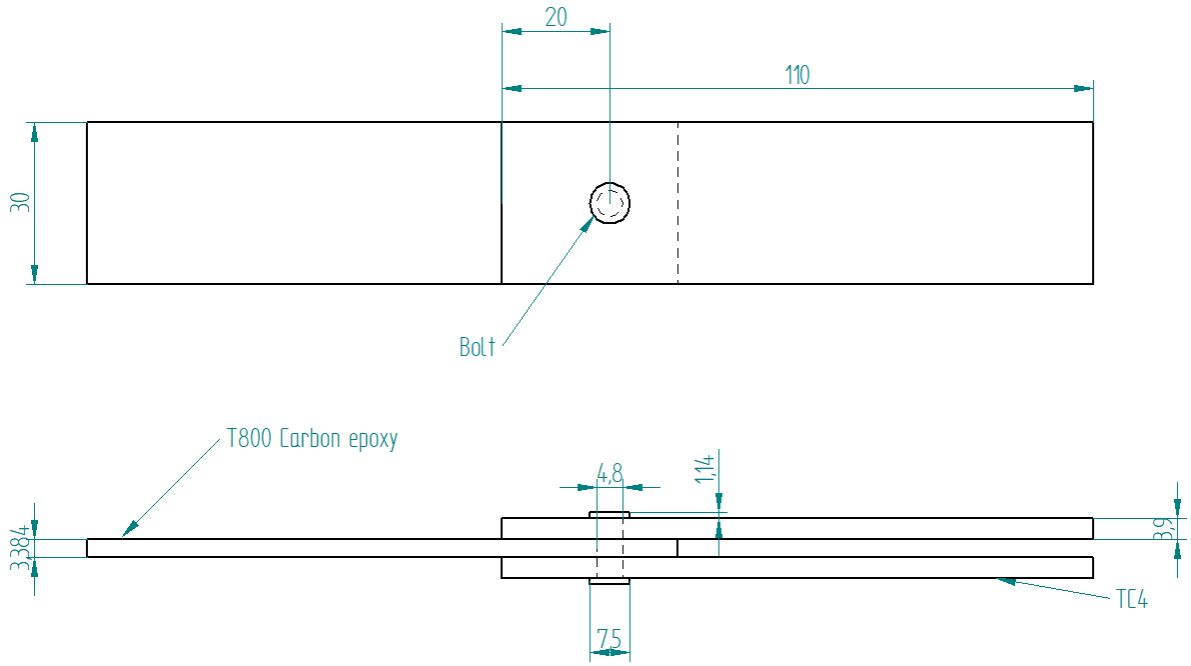

Figure 3.2: DLJ configuration and dimensions (in mm).

3.2.1. Materials properties

During the early modelling stages the materials properties were obtained from a reference paper, where the composite laminate was made from T800 carbon epoxy with orthotropic properties. Each ply has a thickness of 0.188 mm and the stacking sequence is $[+45/-45/0/+45/90/-45/+45/90/-45]_s$ [13]. Table 3.1, Table 3.2 and Table 3.3. present the elastic properties, strength values and fracture toughness of the T800 CFRP, respectively, while Table 3.4. shows the material properties of the metallic parts.

Table 3.1: Orthotropic elastic properties of T800 carbon epoxy [13].

E_{11} (GPa)	$E_{22}=E_{33}$ (GPa)	$G_{12}=G_{13}$ (GPa)	G_{23} (GPa)	$\nu_{12}=\nu_{13}$	ν_{23}
180	8.73	4.49	3.28	0.33	0.48

Table 3.2: Orthotropic strength properties of T800 carbon epoxy [13]**.**

X^T (MPa)	X^C (MPa)	Y^T (MPa)	Y^C (MPa)	$S^L = S^T$ (MPa)
2668	1444	91.8	291	131

Table 3.3: Fracture energies of T800 carbon epoxy.

G_{ft} (N/mm)	G_{fc} (N/mm)	G_{mt} (N/mm)	G_{mc} (N/mm)
130	70	1	5

Table 3.4: Materials properties of the metallic parts [13].

Material	E (GPa)	ν
TC4 plate	105	0.34
HI-Lock Bolt	112	0.31

3.2.2. Modelling in ABAQUS/CAE

Two different approaches were used for this stage: a) "Macro-scale" modelling (one element through the entire laminate thickness) and b) "Meso-scale" modelling (one element through the thickness for each ply). Each individual part that makes the joint was modelled and assembled to make the DLJ. The boundary conditions were chosen to represent the specimen as tested in a universal machine. Thus, the titanium plates are clamped, while, on the CFRP plate, the Y and Z directions are fixed and a tensile displacement in the x-direction is applied, see Figure 3.3. To facilitate the application of the boundary conditions on the CFRP plate for all the modelling strategies, a reference point was created where these displacements were applied. Therefore, all the nodes of the CFRP end face were coupled to this reference point.

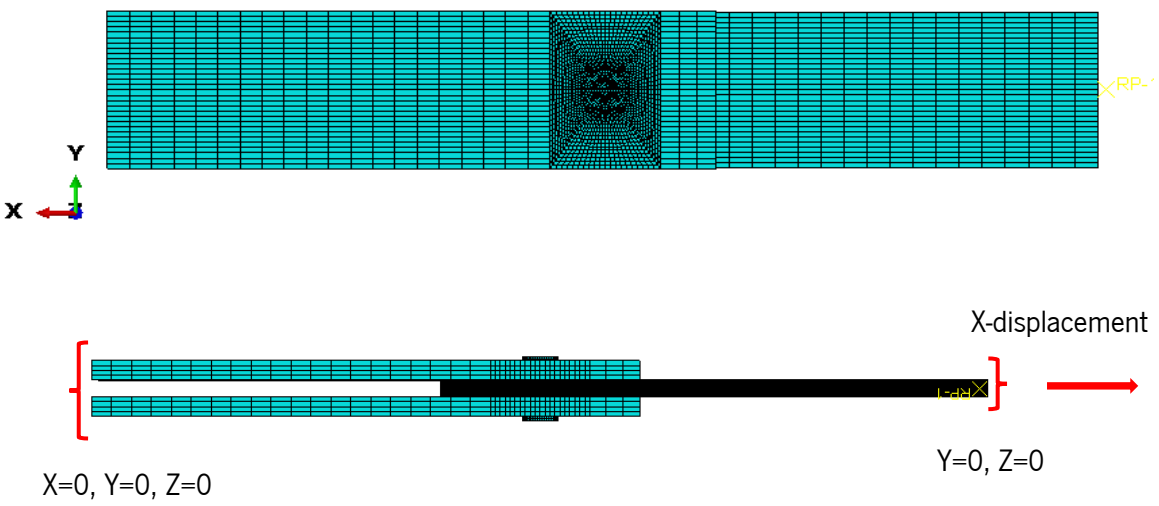

Figure 3.3: Mesh and boundary conditions of the DLJ.

To model the interactions between the components of the double lap single-bolt joint, three contact pairs were defined in ABAQUS. The first contact pair, simulating metal-to-metal interaction, was established between the bolt head and the titanium plate, utilizing surface-to-surface contact with a tangential friction coefficient of 0.1, as defined in [13]. The second contact pair, representing metal-to-composite interaction, was defined for the upper and lower surfaces of the T800 carbon/epoxy composite laminate and the adjacent titanium plates, with a friction coefficient of 0.2 [13]. The third contact pair was assigned to the bolt shank and the hole-bearing surfaces of the composite and titanium plates, also with a friction coefficient of 0.2 [13]. All contact pairs employed a penalty-based contact algorithm with hard contact for normal behaviour, to prevent penetration under compressive loads, and small sliding was assumed to optimize computational efficiency. Surface pairing was explicitly defined, with the composite laminate as the master surface for plate-to-plate contacts and the bolt as the slave surface for hole-to-bolt contacts, ensuring accurate load transfer and stress distribution across the interfaces.

For this exercise three different element types were used to observe the behaviour of the model while loading the composite laminate in tension (in-plane loading): 3D elements (C3D8R), Continuum Shell elements (CS8R) and Continuum Solid Shell elements (CSS8). This prelaminar analysis was done to establish the element that gives the lowest computational time and that is compatible with abaqus built-in Hashin progressive damage model. For the three element types, two different simulations were run: one with linear geometry and another with non-linear geometrical effects to capture large displacements. Linear elasticity was assumed and the implicit solver was employed. The motivation of all this work was

to assess the importance of all these modelling parameters before going deeper in the model with 2 bolts and before doing the uncertainty propagation.

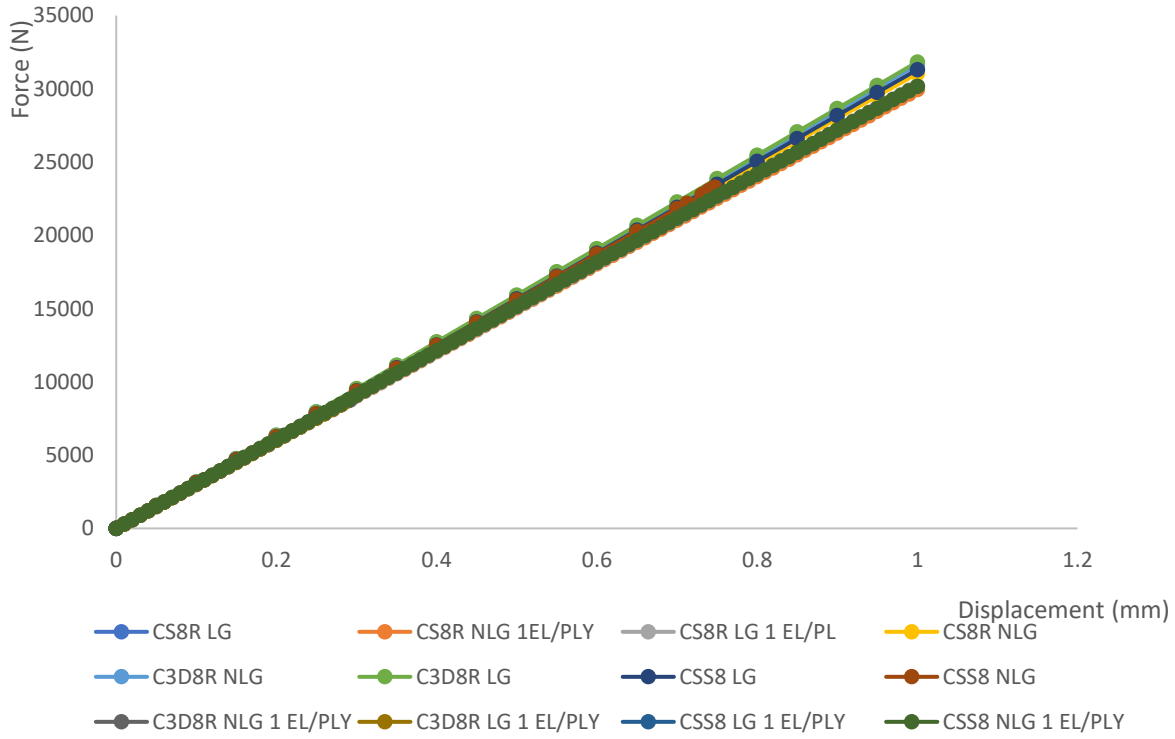

Figure 3.4: Load displacement curve for linear and non-linear geometry with different element types.

Both one element per ply and one element per laminate models behave similarly when no damage occurs, without any exception, as shown in Figure 3.4. From these simulations, computational times were obtained for all the element types with one element per laminate and one element per ply, see Figure 3.5 and Figure 3.6. It can be observed that the continuum shell element had a better performance for both cases. Moreover, it is also compatible with the ABAQUS built-in Hashin damage model, while the others are not. Therefore, it is the element type that will be used in the model validation in this subsection. Notice however, that some analysis done later in Chapter 4 may use again the 3D solid element due to its superior accuracy as it will be explained.

Table 3.5: Computational times and highest load attained from the simulation of one element per laminate model for different element types.

	One element per laminate					
	Linear geometry			**Non-linear geometry**		
	CS8R LG	**C3D8R LG**	**CSS8 LG**	**CS8R NLG**	**C3D8R NLG**	**CSS8 NLG**
Computation time (s)	343	364	466	542	401	1893
Highest step time	1	1	1	1	1	0.747
Maximum load (N)	31263.200	31834.010	31307.300	31034.410	31635.290	23273.900

Table 3.6: Computational times and highest load attained from the simulation of one element per ply model for different elements.

	One element per ply					
	Linear geometry			Non-linear geometry		
	CS8R LG	**C3D8R LG**	**CSS8 LG**	**CS8R NLG**	**C3D8R NLG**	**CSS8 NLG**
Computation time (s)	2570	2845	2670	2798	2748	2650
Highest step time	1	0.282	1	1	0.292	1
Maximum load (N)	30206.700	8505.570	30361.700	29944.260	8790.710	30161.800

3.2.3. Implementation of ABAQUS built-in progressive damage model

The input parameters for Hashin damage initiation are the unidirectional strengths: X^T, X^c, Y^T, Y^c, S^T and S^L; while the inputs for Damage evolution are the fracture toughnesses $G_{ft}^c, G_{fc}^c, G_{mt}^c$ and G_{mc}^c. The values for each of the input parameters were introduced in the ABAQUS property module. These were provided in Tables 3.2 and 3.3. Since these analysis were done in implicit, a viscosity coefficient of 0.001 s was introduced to overcome the convergence issues that arose due to the complexity of the problem.

Figure 3.5 presents the result using Hashin damage model. Introducing this constitutive model caused material non-linearities as expected: the load displacement curve shows a clear linear elastic region, after that a damage initiation at point (a), damage propagation at point (b), and a softening region where the material finally loses its load-bearing capacity (c). It is possible to see that no final failure associated to a catastrophic load drop was obtained, indicating that the joint could still be loaded further. However, it was unneeded to model beyond this point since this exercise focused on defining the modelling and simulation approach for the study using a single element through the thickness of the laminate.

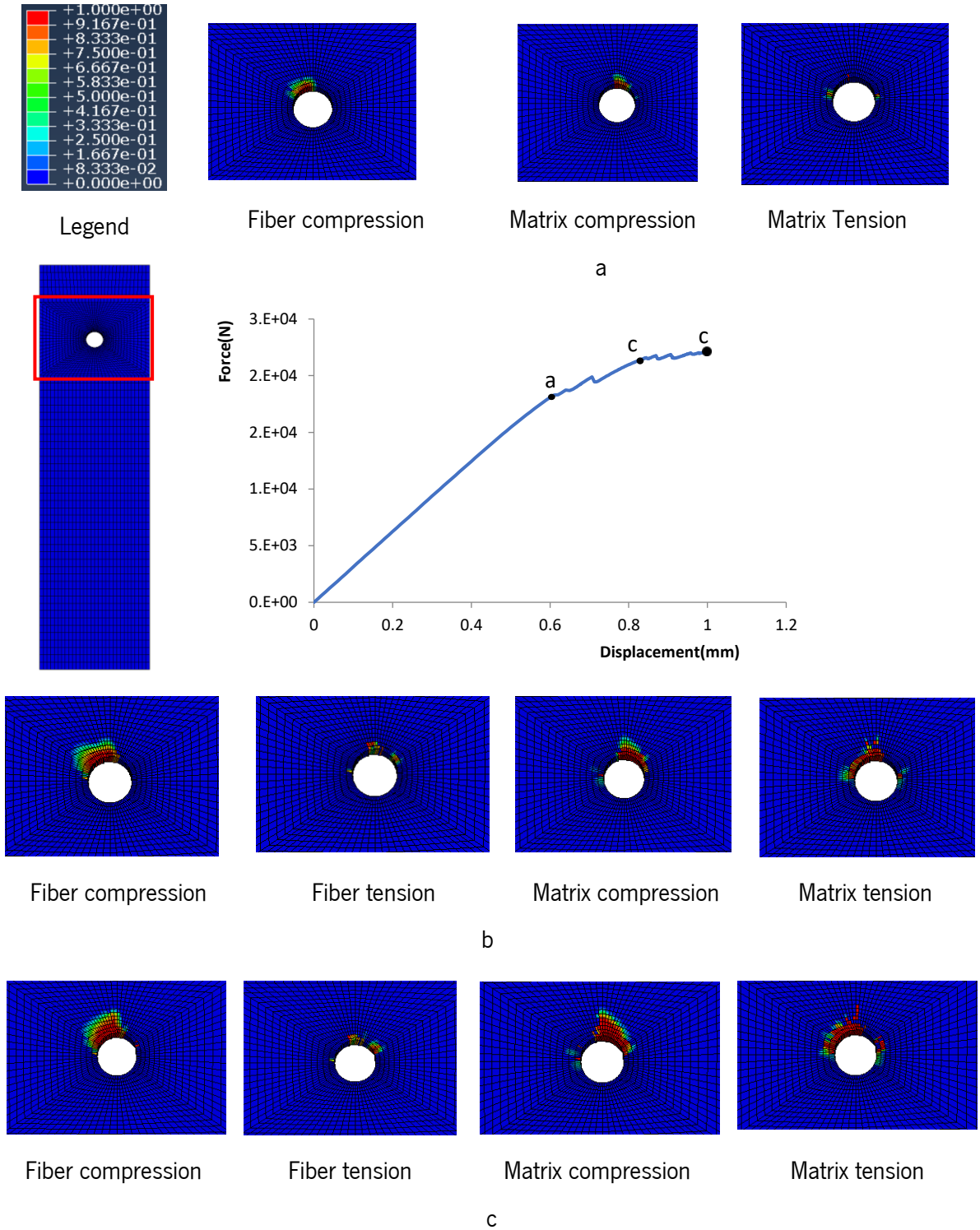

Figure 3.5:Load displacement curve of the DLJ with damage plots.

3.3. Parametrization of the model using Python

During the creation of the model manually using ABAQUS GUI, each click is saved in the .jnl file that can later act as a base to generate a parametric python model. This is done to automate the generation of the model and an input file in the shortest time possible. The script must be parametrized based on the

changing values in the dimensions of the structure so that any change made does not stop the script from running or create an altered model with a totally different model definition. Having a well-parametrized script is important due to its efficiency in producing different models and input files for different parameters without having to do it manually in the GUI. Moreover, for doing an uncertainty quantification analysis, having a proper script is the only way to go. Figure 3.6 shows how long it takes to create a single lap double bolt joint to be used in the case study using a parametric Python script.

```
create_loaded_fastener: bolt_2
13.025
The section "bolt_2_connector_section" has been assigned to 1 wire or attachment line.
The interaction property "contact_property_friction" has been created.
The interaction property "contact_property_frictionless" has been created.
The interaction "contact" has been created.
Warning: Field output is not requested in the following steps:
bolt_preload
The model has been generated
('Total time [min]:', 0.864133334159851)
```

Figure 3.6: time taken to generate the model and an input from the script.

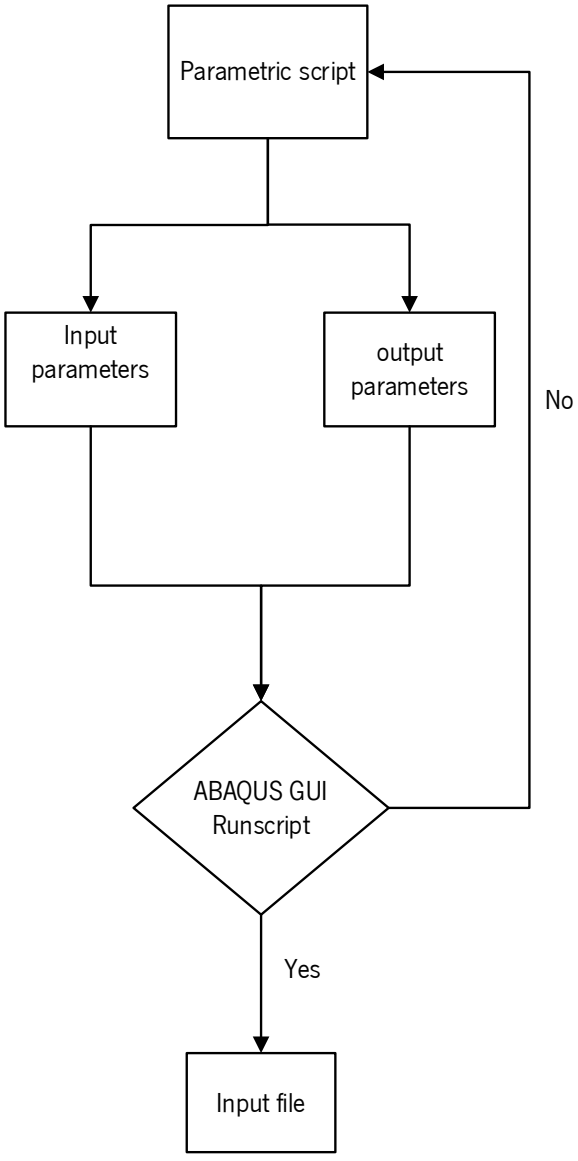

Figure 3.7: Input file generation from a python script.

For the generation of the parametric script, the input parameters that were essential to understand how different tolerances and ply layups affect the structure performance, were: hole misalignments, stacking sequence, bolt-hole tolerances. Besides, all other related parameters (such as specimen dimensions, material data, etc.) were also parametric. By running different simulations with these parameters, the first objective of the project can be achieved. Figure 3.7 shows how the model and the input file can be generated from the parametric script. It is worth mentioning that the script also included a condition to guarantee that no overlapping or components penetrations especially between the bolt and the holes occurred for any misalignment or clearance values.

3.4. Desing of experiments for Uncertainity Quantification

To model the effect of assembly tolerances in composite structures, it is crucial to quantify the uncertainties in a non-deterministic way to create conditions that accurately simulate real-world scenarios. For this reason, a Design of Experiments (DoE) was conducted to generate different models. Two uncertainties are going to be investigated: a) hole to hole misalignment, and b) hole to bolt clearance see Fsigure 3.8. It will be assumed that both have an equal impact on the structure's performance, which is why no sensitivity analysis has been conducted. Although the stacking sequence can also be critical as well as material properties variabilities, these were left out of the scope of this work.

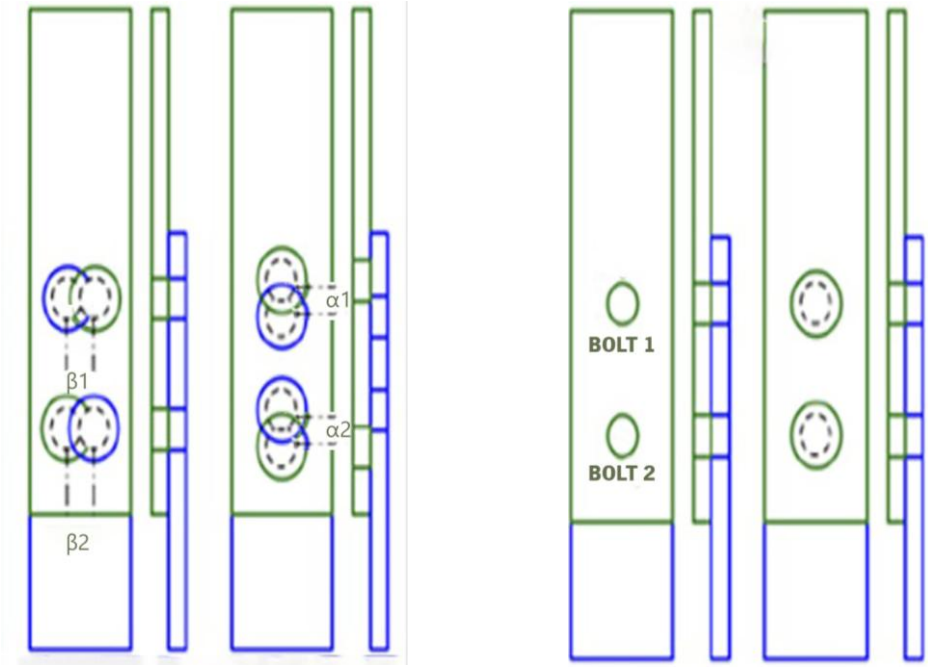

a) Hole to hole misalignment b) Hole to bolt clearance

Figure 3.8: Uncertainties arising from different joint configurations studied

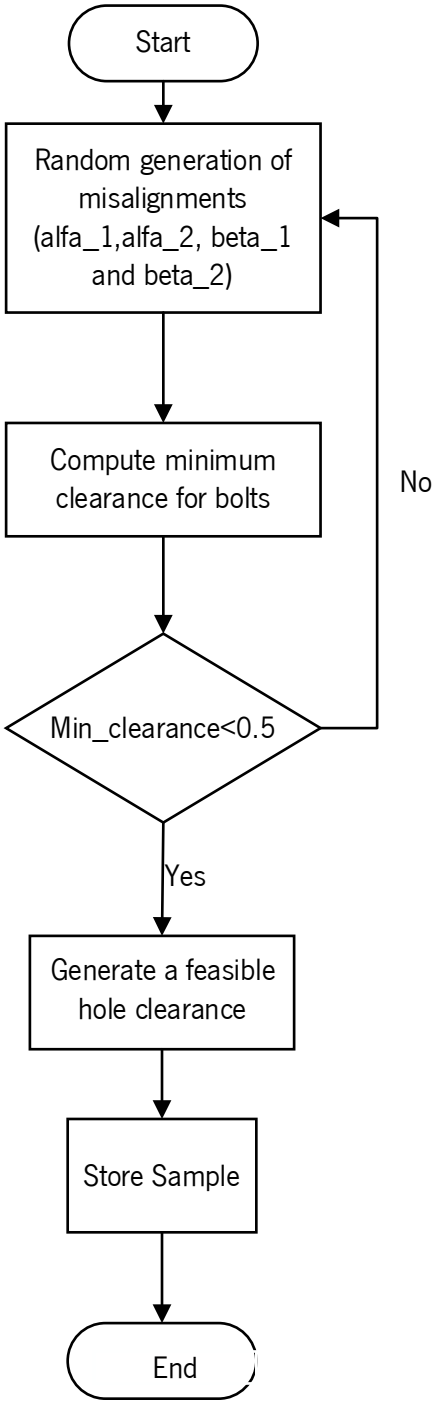

Figure 3.9: Flow chart on the generation for random samples.

The samples are generated using a rejection sampling method with a constraint that min_clearance (minimum bolt to hole clearance) must be equal or less than 0.5 mm. The bolt-hole clearance and misalignments were generated randomly using a Python script with the constraint mentioned above. Samples exceeding this value were discarded (see Figure 3.9), while those within the constraint were stored. In addition, all generated sample guarantee that the bolts go through the holes with no penetration. The obtained DoE will be presented later in Section 4.3.

3.5. Uncertainty Quantification & Management (UQ&M)

To design a composite structure that is representative of real-world conditions, the variabilities (material and geometric variabilities) should be accounted for at the design stage. Using the methodology proposed in the CMH17, B-basis values are computed in order to determine the values of the design allowable while accounting for the variabilities [2, 21]. Figure 3.10 shows the different methods that can be employed to determine the B-value.

In the CMH 17 [2], two approaches are proposed based on whether the data is structured or not structured. With unstructured data, a step-by-step approach is followed to determine whether the data follows a Weibull, Normal or logarithmical distribution. This methodology also suggests that a test for goodness fit is performed for these distributions in order to establish the approach to be used in the computation of B-values. If the OSL (Observed Significance Level) has a value greater than 0.05, the B-value is computed using the Weibull distribution approach, while if the OSL for the Weibull distribution is less than 0.05 and the OSL for the Normal distribution is greater than 0.05, the B-value is computed using the Normal distribution approach. For the cases where the OSL for both Weibull and Normal distribution is less than 0.05, the Log-normal approach is used to compute the B-value. If none of the OSL is greater than 0.05, then it is recommended to use the non-parametric procedures, in which the B-value can be computed using an approach for large samples ($n>28$) and Hanson-Koopmans for samples ($n<28$) [2].

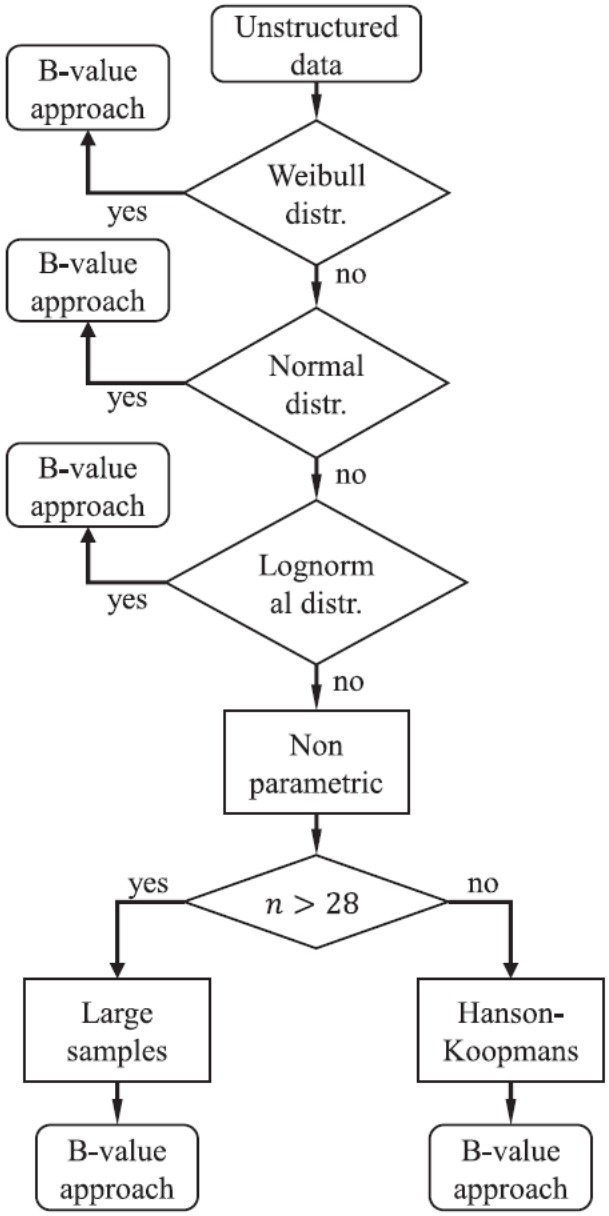

Figure 3.10: Flow chart of the steps taken to calculate the B-value using the CMH17 methodology [21].

3.6. Computing the knock down factors

Following the proposed approach in section 3.5, a B-basis value can be estimated with a 95% lower confidence limit. With the B-value known, the knock down value (KDF) can be obtained by dividing the B-value with a reference value, following Eq. (3.1)

$$KDF = \frac{b\ value}{Refrence\ value} \tag{3.1}$$

The reference value considered for this study will be the ideal values of the joint without clearances and misalignments.

4. CHAPTER 4: CASE STUDY (SINGLE LAP DOUBLE BOLT JOINT)

The presented methodology can be applied to a case study to compute the knock down factors. In this study, the case will be a single lap double bolt joint. This configuration was chosen because it is more representative of the real-world structures with bolted joints since they are always made of multiple bolts. In these joints, the overall performance is not only affected by the material strength, but also by the assembly quality that results from geometric tolerances, such as the bolt to hole clearances and hole to hole misalignments.

4.1. Definition of simulation and modelling approach

A robust finite element model was developed using the ABAQUS explicit solver. While the previous explorative simulations in Chapter 3 used implicit, this chapter switched to explicit. This was motivated by the fact that with implicit it is challenging, if not impossible, to model a large portion of damage without having convergence issues.

In addition, as introduced before, the linear behaviour comparing different models was quite similar, although of course, the softening behaviour will be different depending on the model complexity, as well as the computational time. Therefore, it will also be further explored the difference provided by two extreme modelling strategies of different complexity:

- **Macro-scale modelling:** this strategy is the simplest one. It consists in using one element through the full laminate thickness, together with abaqus built-in Hashin damage model and continuum shell elements CS8R. While this strategy may lose some details to capture the full damage development, it will be computationally efficient and may be an excellent candidate to estimate design allowables.
- **Meso-scale modelling:** this strategy is the most complex and detailed one. It consists in using three elements through each ply thickness, together with 3D solid elements C3D8R. Since the ABAQUS built-in Hashin model is not compatible with 3D solids, material non-linearities were introduced through a user subroutine developed by the AMADE research group, referred as “PG3D”, see the work from Cózar et al. [25]. While

in the literature it is common to mesh each ply with a single element through the thickness, here we will mesh with 3. The motivation behind this is because it allows to have a better stress discretization through the thickness, avoiding having to input in-situ strength properties. In addition, thanks to the fact that this constitutive model is fully 3D, this mesh discretisation allows to capture delamination without the use of cohesive interfaces, since the cracks can grow in the elements at the vicinity of the plies.

For the sake of brevity, other modelling strategies explored in Chapter 3 were left out of this work. The dimensions of the composite plates are provided as a function of the nominal diameter of the bolt, 6.35 mm, to facilitate the generation of a parametric Python script, and the configuration is a single lap shear double bolt joint as shown in Figure 4.1. The specimen plates are all made of CFRP material, while the bolts are made of Titanium. In order to counteract the moments in the assembly when pulling, the specimen contains doublers on both ends of the joint, which are also of the same CFRP.

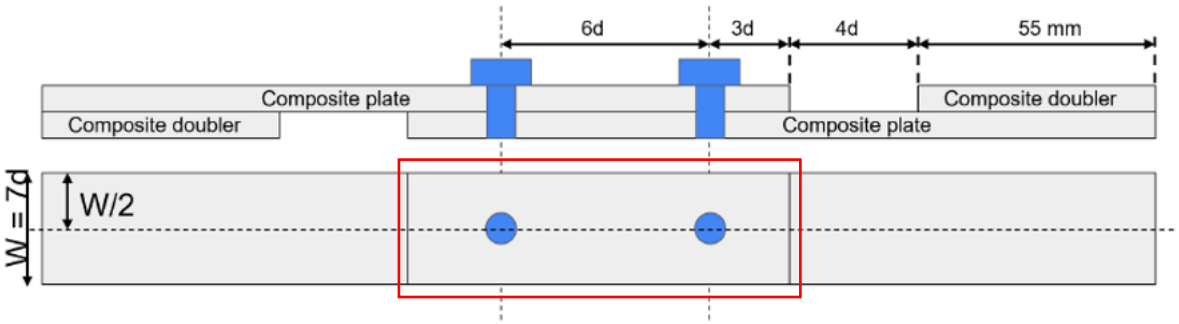

Figure 4.1: SLJ double bolt configuration and dimensions, where "d" is the bolt nominal diameter.

4.1.1. Materials properties

The CFRP material consisted in IMA/M21E, which is a widely employed aeronautical material. The corresponding UD elastic properties, the strength and the fracture toughness, needed to perform the simulations accounting damage behaviour, are described in Table 4.1. The stacking sequence is [45/0/135/90]2s, and each ply has a nominal thickness of 0.184 mm.

The bolts are made of Titanium alloy, whose properties are described in Table 4.1. Since plasticity is expected to develop in the bolts due to the high localized contact stresses, plasticity behavior was also added into the bolts by taking advantage of Abaqus isotropic hardening model.

Table 4.1: Necessary input properties for the model

	Description	Symbol
Elastic properties	Longitudinal Young's modulus of the CFRP ply	E_{11}
	Transverse Young's modulus of the CFRP ply	E_{22}
	In-plane Shear's modulus of the CFRP ply	G_{12},G_{13}
	Out-of-plane Shear's modulus of the CFRP ply	G_{23}
	In-plane Poisson's ratio for the CFRP ply	ν_{12}, ν_{13}
	Out-of-plane Poisson's ratio for the CFRP ply	ν_{23}
Strength	Unidirectional longitudinal tensile strength	X^T
	Unidirectional longitudinal compressive strength	X^C
	Unidirectional transverse tensile strength	Y^T
	Unidirectional transverse compressive strength	Y^C
Fracture toughness	Longitudinal tensile fracture toughness	G_{ft}
	Longitudinal compressive fracture toughness	G_{fc}
	Transverse tensile fracture toughness	G_{mt}
	Transverse compressive fracture toughness	G_{mc}
Titanium bots	Elastic modulus of the metallic parts	E
	Poisson's ratio of the metallic parts	ν

4.1.2. Model generation

A parametric Python script compatible with ABAQUS scripting, developed previously at AMADE research group, was used to generate the models for this study. It was based on the geometry and parameters shown in Figure 4.1. It was created to enable the timely creation of models and the generation of input files for simulation runs. In the Python script, certain variables are modified to select one modelling strategy or the other.

The doublers were meshed with 3D solid elements and with three elements through the full thickness with a coarse mesh, since they do not play any role on the damage development. They were also assigned elastic properties. The composite plates that make up the structure have a zone of interest, as shown in Figure 4.1 surrounded by a red rectangle, where the damage is expected to develop. Hence, the damage properties were applied only in this region. This zone has a refined mesh size of 0.5 mm (which is small enough to avoid any snap-back from the constitutive damage models). Depending on the modelling strategy, this region employed either: a) one element per laminate and continuum shell elements with

reduced integration (SC8R); or b) three elements per ply and 3D solid elements with reduced integration (C3D8R), see Figure 4.2. The remaining composite part makes use of 3D solid elements with a coarse mesh size without compromising the aspect ratio, with three elements through the thickness as done with the doublers. Partitions were made to make sure the mesh is well structured. Surface to surface tie constraints were used to bond the refined region of interest with the remaining coarse elastic parts and with the doublers.

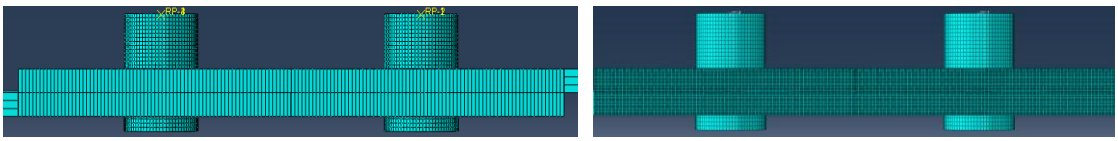

a) b)

Figure 4.2: Modelling approach for the bolted area. a) Macro-scale modelling (1 element through the full laminate thickness) and b) Meso-scale modelling (3 elements per ply).

The bolts and the nuts were also meshed with a mesh size of 0.5 mm (to be as much coincident as possible compared with the composite part) and 3D solid elements C3D8R see figure 4.3

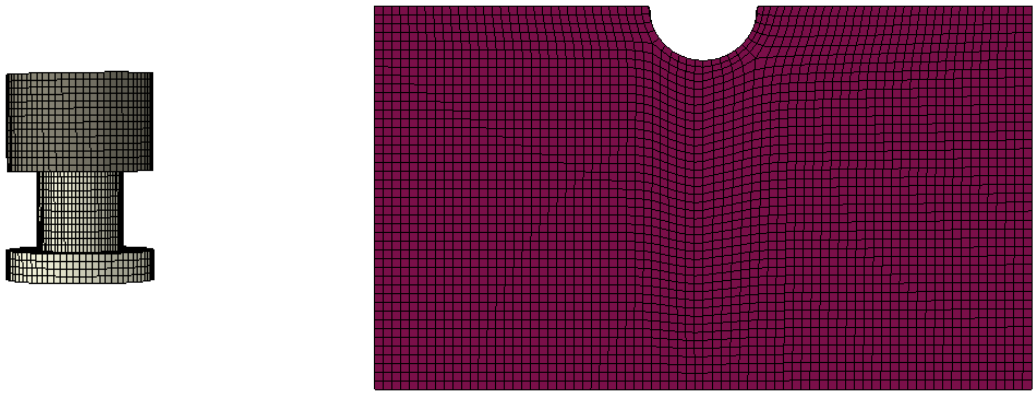

Figure 4.3: Bolt&Nut, and hole mesh.

The simulation consists of 2 steps. In the first step, the assembly is preloaded by tightening the two bolts. To do so, the strategy presented in Cózar et al. was employed [26]. In brief, a virtual connector element (CONN2D2 Abaqus element) with no stiffness is created to link the bolt with the nut. Then, a compressive axial load equal to the desired preload (in this case 5904.16 N) is applied to the connector using a smooth step, while the left and right regions shown with the red rectangle in Figure 4.4 were clamped. This region corresponds to all the length of the doublers. After the first step, the second step starts, where the virtual test is preformed. In this step, the length of the connector is kept fixed and it's axial load is removed. This approach allows to keep the bolt preload as is at the beginning of the step, but also allows the parts to deform freely, altering the contact force between parts as naturally needed to reach equilibrium. In addition, assembly is clamped on the left side, whereas a tensile displacement is applied in the x-direction from the right side of joint as it can be seen in Figure 4.4. The loading rate was set to 65 mm/s, which is

much higher than typical experimental tests. However, it is small enough for making sure the total kinetic energy is negligible compared to the total internal energy to be considered as quasi-static loading.

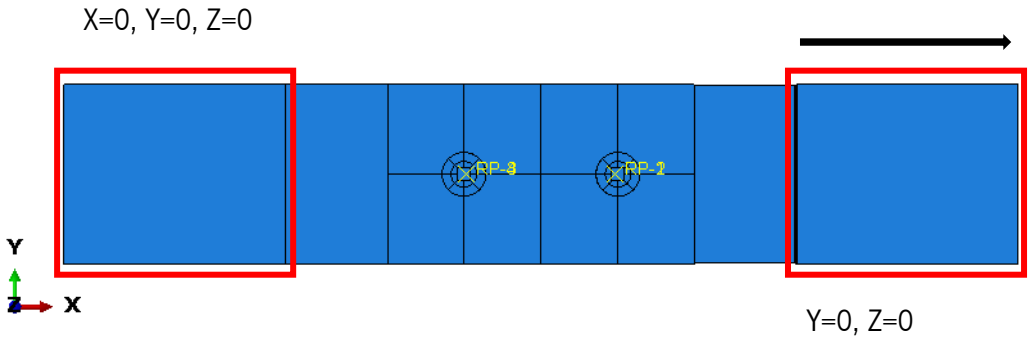

Figure 4.4: Boundary conditions for the SLJ.

To simulate the interaction between the different parts, the powerful general contact algorithm of ABAQUS was employed. Thus, this allows to capture dynamically the contact between any surfaces that touch during the analysis. As a global property assignment, penalty method with hard contact and a friction coefficient of 0.1 was assigned everywhere, except between the nut and the bolt, where the friction coefficient was specifically set to 0.

4.1.3. Tolerances and Nominal Configurations

Firstly, a deterministic approach was used to quantify uncertainties and comparing the two modelling strategies, as shown in Table 4.2. Each uncertainty affects the assembly differently and, therefore, produces a distinct load displacement curve that fully represents what could happen in a real structure with that configuration. The cases labeled with "A" do not have any misalignment. The number accompanying the letter indicates the oversize value. The cases labelled with a letter other than "A" have a misalignment, and all these cases have a clearance of 0.5 mm to guarantee that the bolt goes through all the hole without penetration. The misalignment can be in the longitudinal direction (alfa) or in the transverse direction (beta), and may be in bolt 1 or 2. Thus, there are 4 possible misalignment values: alfa_1, alfa_2, beta_1, and beta_2. Half of the value is applied to the top plate, and the negative of the other half is applied to the bottom plate. For example, if alfa_1 = 0.5 mm, this means that in bolt 1, the total misalignment in the longitudinal direction is 0.5 mm. The top hole centre is misaligned 0.25 mm in the length direction in the positive direction, while the bottom hole centre is misaligned 0.25 mm in the other direction.

Table 4.2: Nominal configurations of single lap double bolt joint.

Specimen label	Nominal holes Oversize [mm]	Hole misalignments [mm]			
		alfa_1	alfa_2	beta_1	beta_2
A0	0	0	0	0	0
A3	0.3	0	0	0	0
A5	0.5	0	0	0	0
B5	0.5	0.5	0	0	0
C5	0.5	-0.5	0	0	0
D5	0.5	0	0	0.5	0
E5	0.5	0	0	0.5	-0.5
F5	0.5	-0.5	0.5	0	0

After quantifying the uncertainty and running simulations with them, it is essential to note the computational time for each configuration and model type, as this influence which modelling strategy is to be used in the non-deterministic uncertainty propagation later. The computational times for all the configurations are displayed in Table 4.3.

Table 4.3: computational times in seconds for the two modelling strategies.

Specimen label	Computational time [hrs. mins]	
	Hashin	PG3D
A0	6. 42	22.39
A3	6.0	12.21
A5	5.56	19.18
B5	15.33	30.0
C5	18.47	24.36
D5	13.39	29.15
E5	18.59	35.53
F5	16.37	26.06

4.2. Results for nominal configurations

All the nominal joint configurations were run with the 2 modelling strategies presented. Results are shown separately for clearances (A5, A3, and A5) and for misalignments (B5, C5, D5, E5, and F5).

4.2.1. Results for configurations A0, A3 and A5

All the joint configurations behave similarly, with the joint configuration A0 showing no delay in the load-up take, see Figure 4.55a. This is because the force is directly applied to the bearing surfaces of the composite laminate due to the absence of clearance between bolt and hole. For A3 and A5, a visible delay in the load-up take is observed, as evidenced by a 0.3 mm and 0.5 mm sliding, respectively, corresponding to the clearance values, as shown in Figure 4.55b,c. Due to the clearances in configuration A3 and A5, there is a reduction in the surface area of contact between the bolt and the bearing surfaces of the plates, which reduces the load-bearing capacity for the two configurations in comparison to A0, which has no clearance. Therefore, it can be established that the increase in clearance reduces the joint strength.

What cannot go unnoticed is the difference in the prediction between the two models. During the elastic region, both models are evenly matched. Moreover, the onset of damage is also very much alike between both models. However, after the damage onset the model with three elements per laminate shows a continuous softening and thus, predicts a loose of capacity to bear the load. Oppositely, for the one element per laminate, a hardening phase can be observed because once the damage initiates, the pristine parts of the matrix and fibres can bear the load. Due to the lack of experimental data, it is currently not possible to clarify which of the 2 cases is giving the best prediction, although the model with 3 elements per ply is more robust and uses a more advanced constitutive damage model, so it may be closer to reality. In any case, the damage onset is nearly identical for both approaches. Thus, focusing on this point, both methodologies can indistinctly be used.

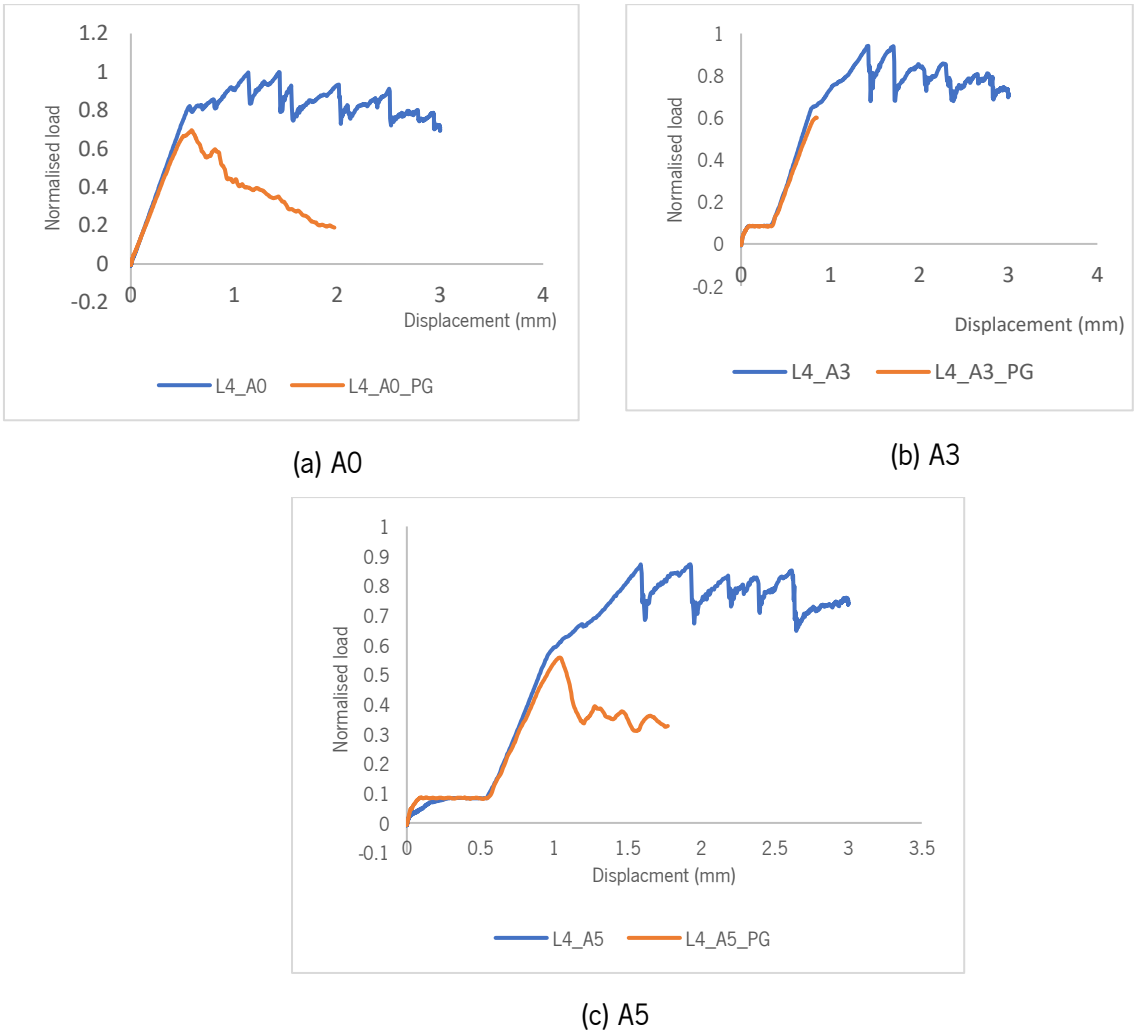

Figure 4.5: Load displacement curves for Configuration A0, A3, and A5.

From the meso-scale model (three elements per ply), it is possible to visualise the extent to which both fibres and matrix are damaged at the end of the simulations by requesting for SDV_DL and SDV_DST respectively from Visualisation. With the quasi-isotropic laminates, while loading longitudinally, the most critical ply is the 90° ply. Apart from A3, that aborted prematurely due to excessive distortion of elements, the other two configurations A0 and A5 showed similarities in what is to be expected from a quasi-isotropic laminate. The 90° ply shows matrix cracking and what could be interpreted as delamination around the whole due to the stress concentrations and the orientation of the 90° plies for both the bottom and top plates for the lap joint as it can be seen in Figure 4.6 and 4.6. Overall, it can be established that in quasi-isotropic laminates loaded longitudinally, the 90° plies are the weakest.

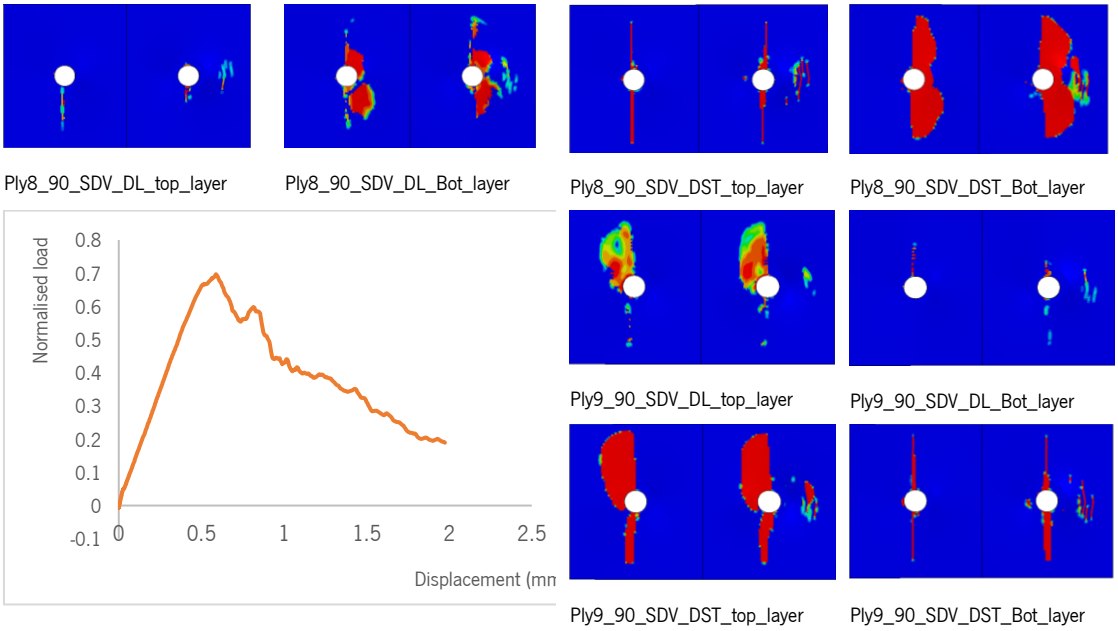

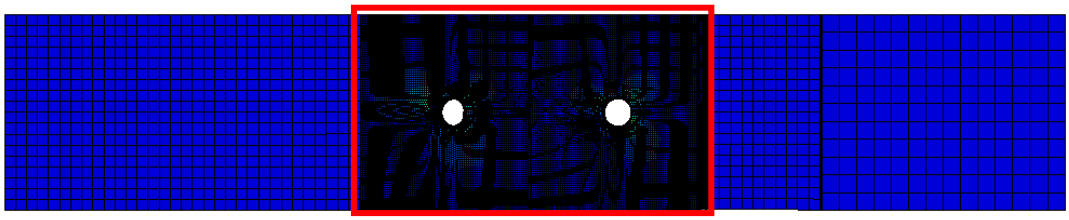

Figure 4.6: Bottom_plate A0 configuration, ply 8 and 9 damage plots at load drop.

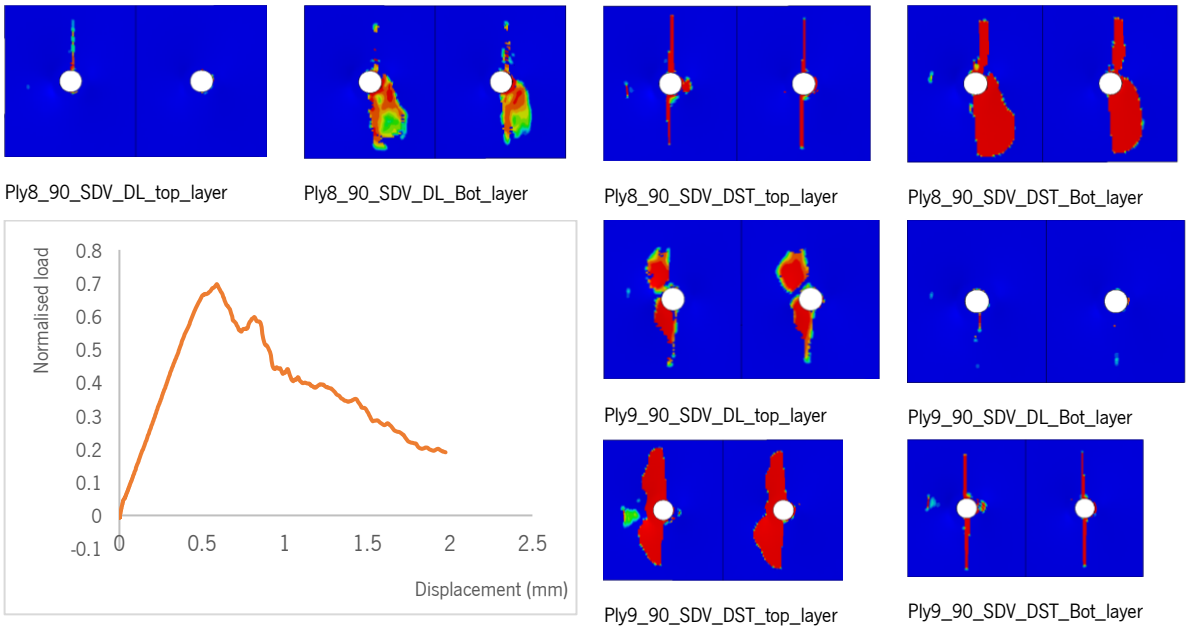

Figure 4.7: Top_plate A0 configuration, ply 8 and 9 damage plots at first load drop.

4.2.2. Results for configurations with misalignment

In bolted structures, a slight misalignment of the holes creates residual forces in the joint, which reduces its overall load-bearing capacity, as will be shown in this section.

Specimen configuration B5

In this configuration, there is a misalignment of 0.5 mm in the x direction between the top and bottom plates in the right hole, as shown in Figure 4.8 detail B.

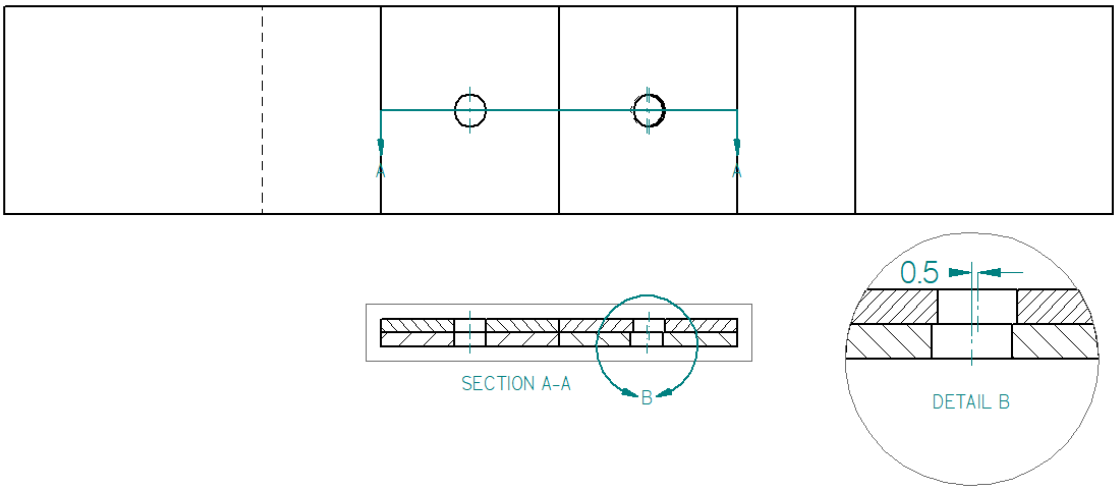

Figure 4.8: Detail B for the misalignment between top and bottom plate in the right-hand side bolt.

From this misalignment and an initial clearance of 0.5 mm, upon loading there is sliding in all bolts and the load increases linearly till the first knee point at approximately a displacement of 1 mm as shown in Figure 4.9. This is due to the misalignment between top and bottom plate in the right holes that makes it in a way that the top plate right hole seems to have a clearance of 1 mm, this makes the bearing surface of the top plate left hole work together with the two bearing surfaces in the bottom plate. As a result, the area in contact with the bolts is reduced, hence reducing the overall joint strength. Again, the two modelling strategies show different behaviour but the onset of damage (first knee point) is the same.

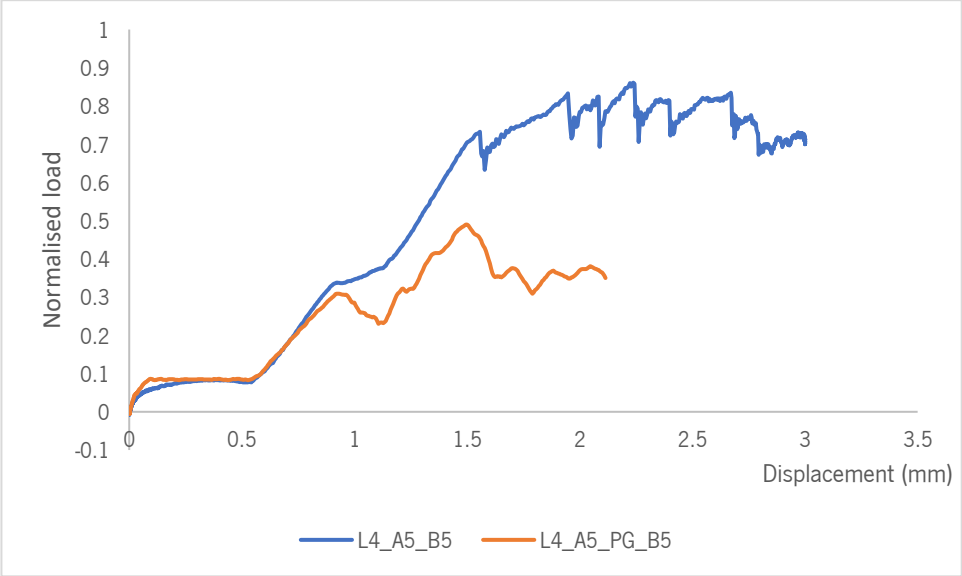

Figure 4.9: Load displacement curve for misalignment configuration B5.

A visualisation of damage in the bottom plate shows both bearing surfaces share the load from the beginning of the loading as shown in Figure 4.10.

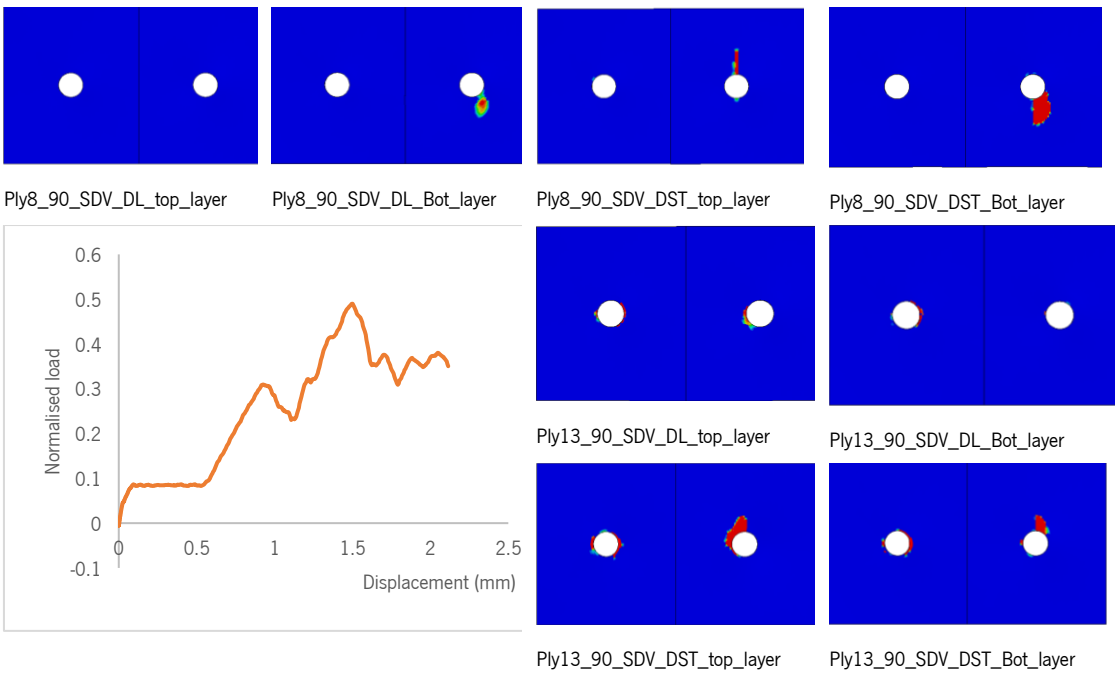

Figure 4.10: Bottom_plate B5 configuration, ply 8 and 13 damage plots at the peak load.

Because of the misalignment, more damage can be observed in the top plate than in the bottom plate due to load being carried by the left bolt at the start of loading. In Figure 4.11 more bearing damage can be observed in the left bearing surface compared to the right bearing surface.

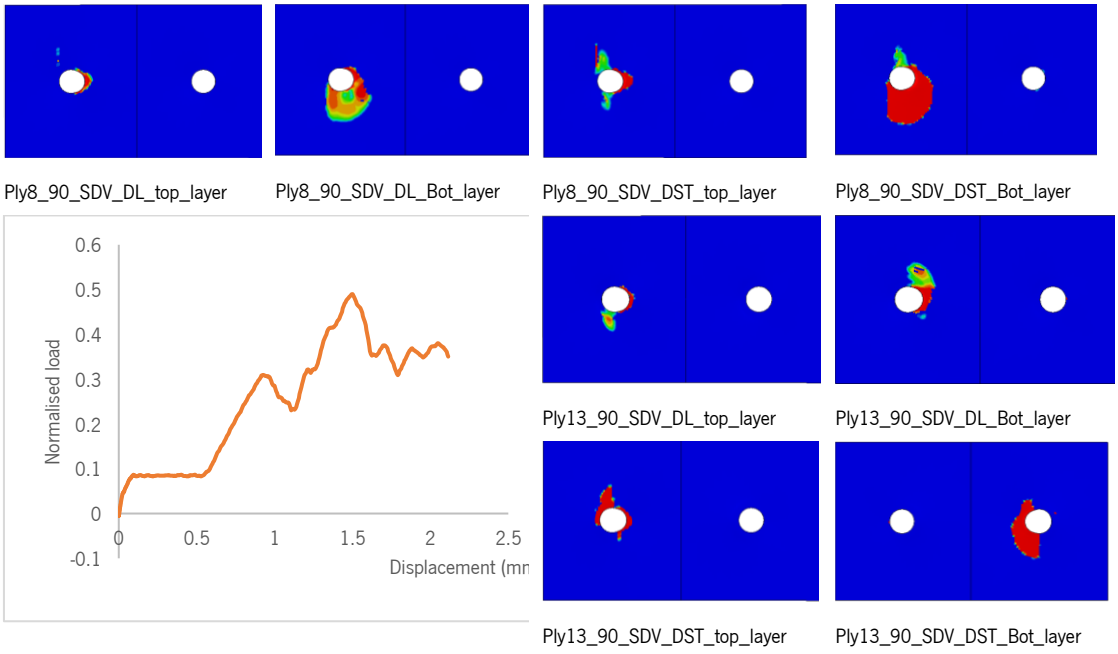

Figure 4.11: Top_plate B5 configuration, ply 8 and 13 damage plots at the peak load.

Specimen configuration C5

Similar to specimen B5, the misalignment occurs between the top and bottom plates, specifically at the right holes of the joint, with a -0.5 mm shift in the x direction. Unlike other configurations with clearances, this type of misalignment prevents sliding because the bearing surface of the top plate's right hole is directly in contact with the bolt shank, allowing load transfer to the joint. However, since only one of the four bearing surfaces carries the load, the initial load drops at a low load magnitude at a displacement of about 0.5 mm, as shown in Figure 4.12. After that, the load increases as all four bearing surfaces share the load. The two modelling strategies are again in good agreement in the prediction of the knee point, but not the rest.

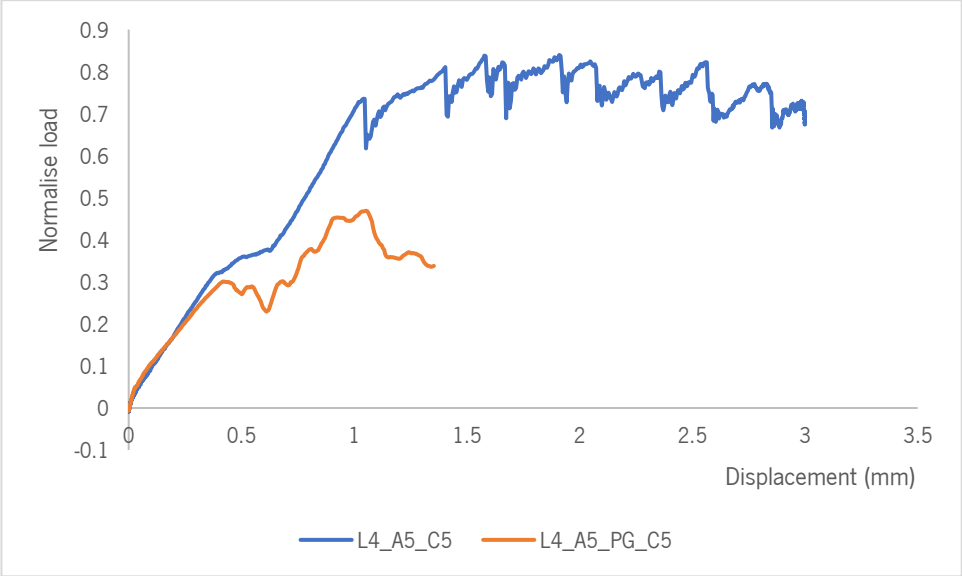

Figure 4.12: load displacement curve for the misalignment configuration C5.

Since there is an offset of -0.5 mm between the top and the bottom plates on the right-hand holes, the joint doesn't seem to have a clearance. Thus, the overall bolt free movement is reduced within the bottom plate holes having no apparent damage in the zone surrounding the left hole compared to the right hole, which carried most of the loading at the beginning until a displacement about 0.5 mm, see Figure 4.13.

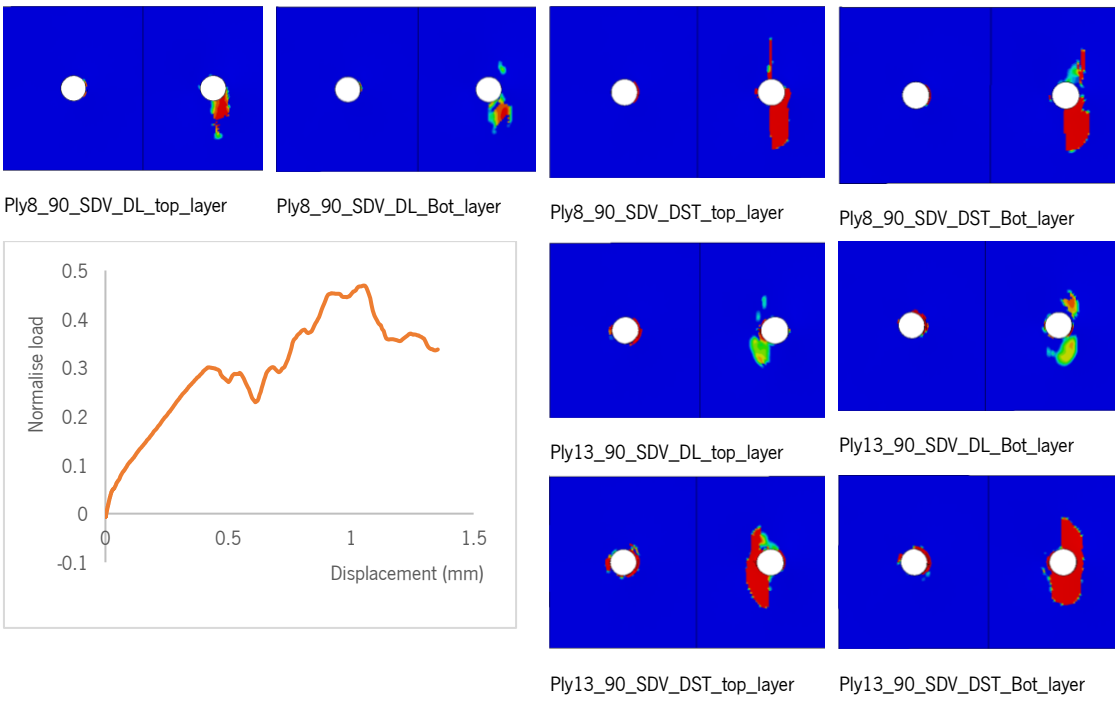

Figure 4.13: Bottom_plate C5 configuration, ply 8 and 13 damage plots at the peak load drop.

On the contrary in the top plate, due to non-symmetric loading and the free movement of the left bolt due to the clearance, there is a significant damage in the bearing surface of the left hole compared to the

right hole (Figure 4.14). This is due to the bending of the plates at the left-hand side that is caused by the non-symmetric loading present in single lap shear joint.

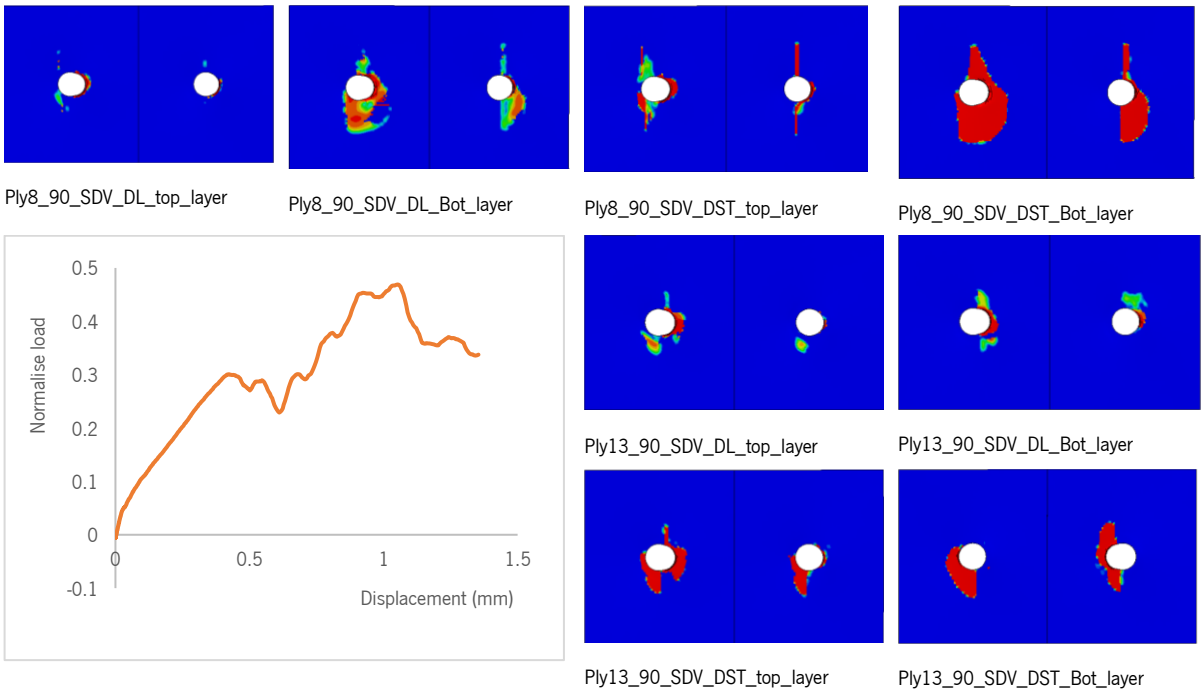

Figure 4.14: Top_plate C5 configuration, ply 8 and 13 damage plots at the peak load drop.

Specimen configuration D5

In this configuration, a 0.5 mm misalignment is introduced between the top and bottom plate holes in the y-direction (transverse axis). This is well displayed in the detail view in Figure 4.15.

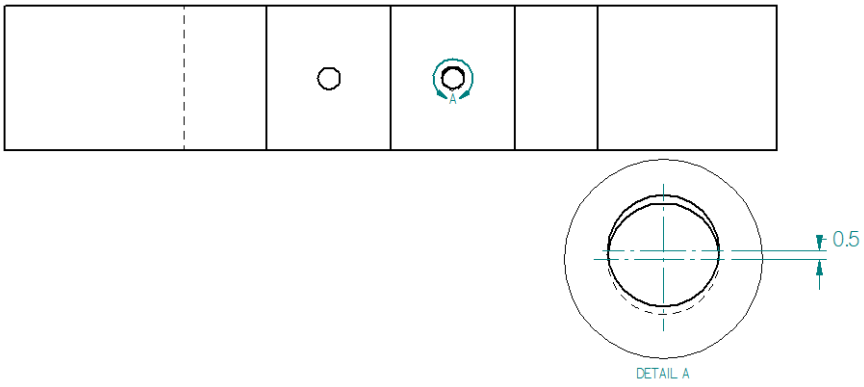

Figure 4.15: Detailed view of the misalignment between top and bottom plate right holes in the Y-direction.

This misalignment does not necessarily reduce the joint stiffness, as it can be seen in the load displacement curve in Figure 4.16. Due to the misalignment shown in detail A of Figure 4.15, the bolt is not in contact evenly with the bearing surface of the right hole, therefore creating a localised stress concentration zone on its bearing surface. This leads to the reduction of joint stiffness, first knee point load

and the first load drop. Again, the two model strategies agree well on the predictions until the damage onset.

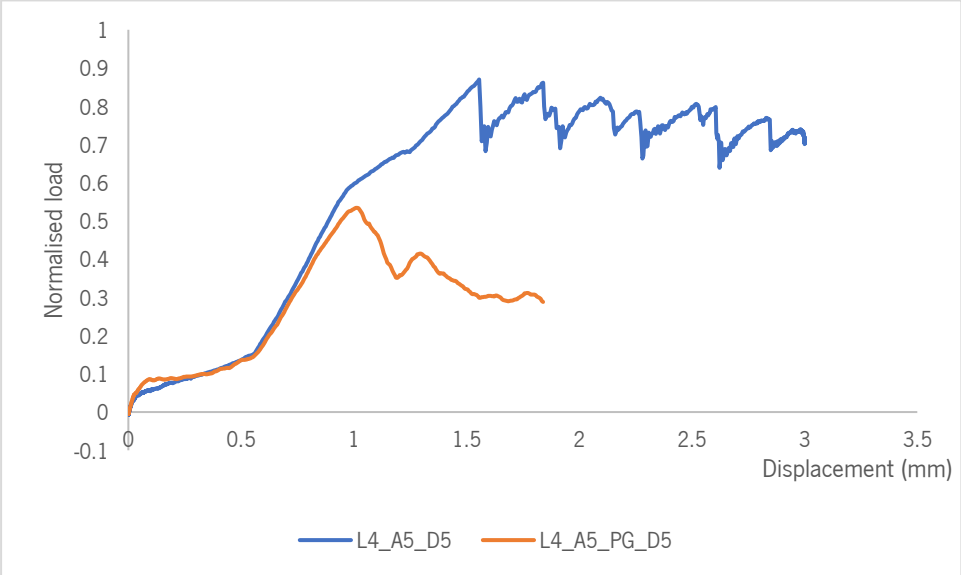

Figure 4.16: Load displacement curves of configuration D5.

Since the displacement is applied on the bottom plate having the top plate fixed, this misalignment alters the load distribution at an angle in the holes with the misalignments, as can be seen from the oval shaped failure for the right hand holes in both Figures 4.17 and 4.18 showing the damages in plies 9 and 13. A bearing damage (oval-shaped) directed at an angle can be observed in the right holes in both the top and bottom plates.

It is important to note that with this misalignment the area surrounding the right hole suffers more significant damage due to the change in load distribution that is introduced; this can be well seen in Figure 4.17, showing the damages in the bottom plate, where the area surrounding the left hole seems undamaged due to a slightly larger surface area of contact with the bolt.

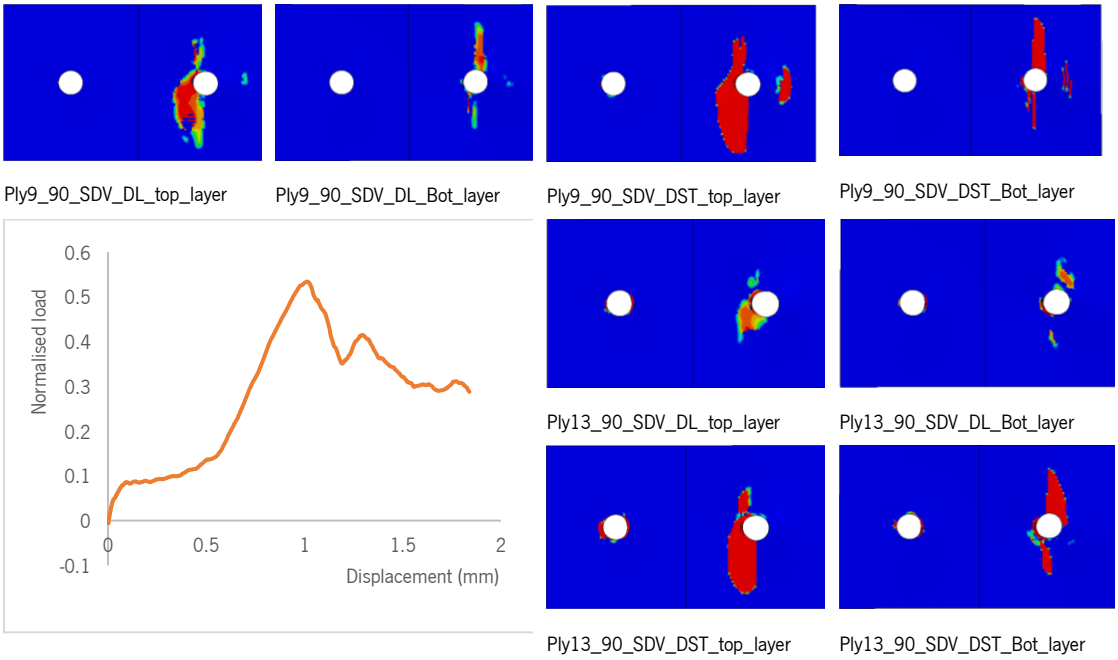

Figure 4.17: Bottom_plate D5 configuration, ply 9 and 13 damage plots at the first load drop.

In the top plate, the damage is minimal, primarily because most of it occurred in the left bearing surface hole. This damage is due to bending introduced by asymmetric loading in the joint and the clearance that allows the bolt's free movement, creating a stress concentration around that area. The area of focus is on the right bolt because with the misalignment in the y-direction, the bearing failure occurs at an angle, and it is the same as what can be observed in the right hole of the bottom plate.

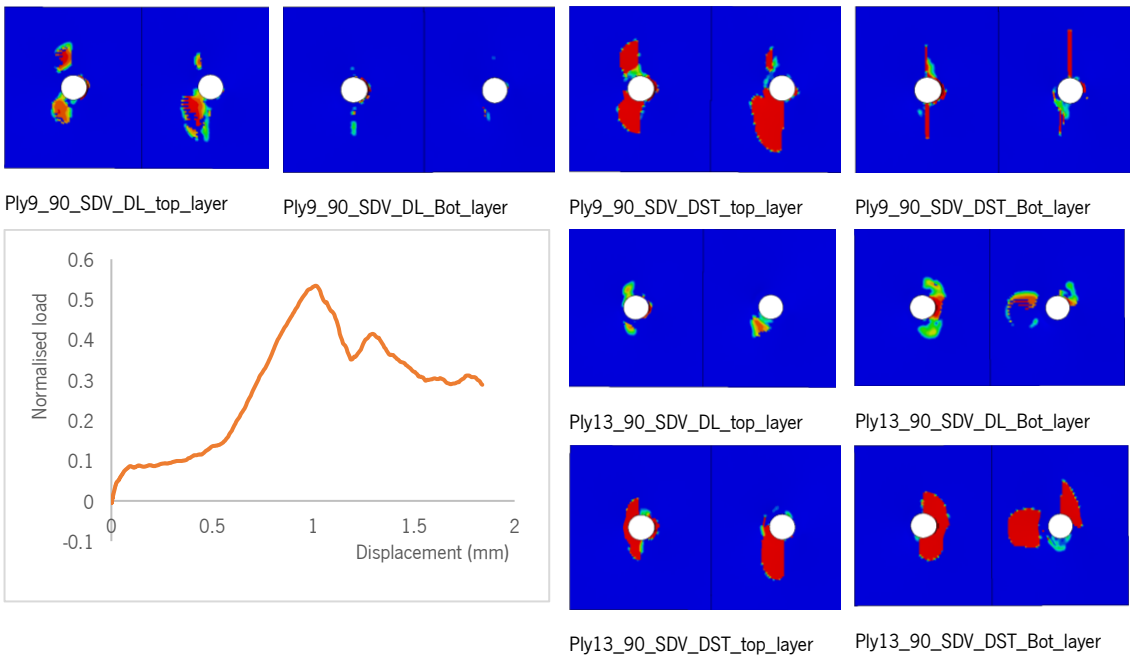

Figure 4.18: Top_plate D5 configuration, ply 9 and 13 damage plots at the first load drop.

Specimen configuration E5

In this configuration, both the left hole and the right holes have opposite misalignments between the bottom and the top plate, as indicated by Details A and B in Figure 4.19. The misalignment in Detail A is -0.5 mm, while in Detail B is 0.5 mm, both being in the y direction.

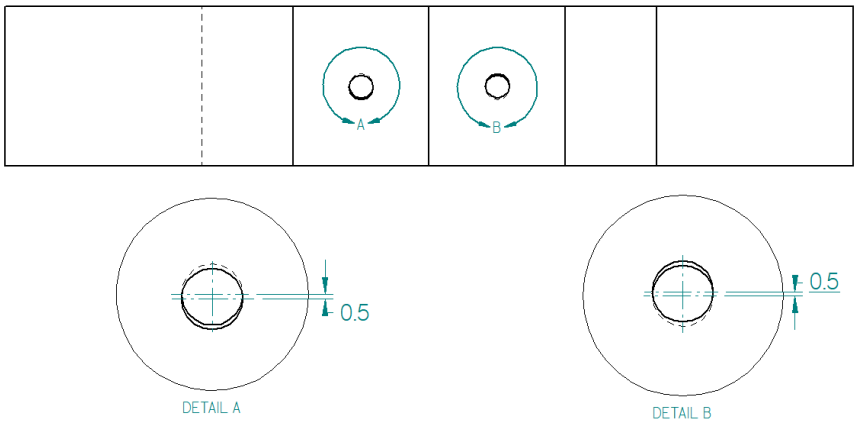

Figure 4.19: Specimen E5 configuration of misalignments.

In this kind of configuration, there is a significant reduction in the load bearing capacity of the joint, due to reduction in the surface area of contact between the bolt shank and the bearing surface of the two holes. This is observed on the load displacement curve (Figure 4.20) where the first load drop is much lower compared to the other configuration with only a misalignment on one side or cases with just a clearance. Again, the behaviour between the 2 modelling strategies is reasonably matched until the damage onset.

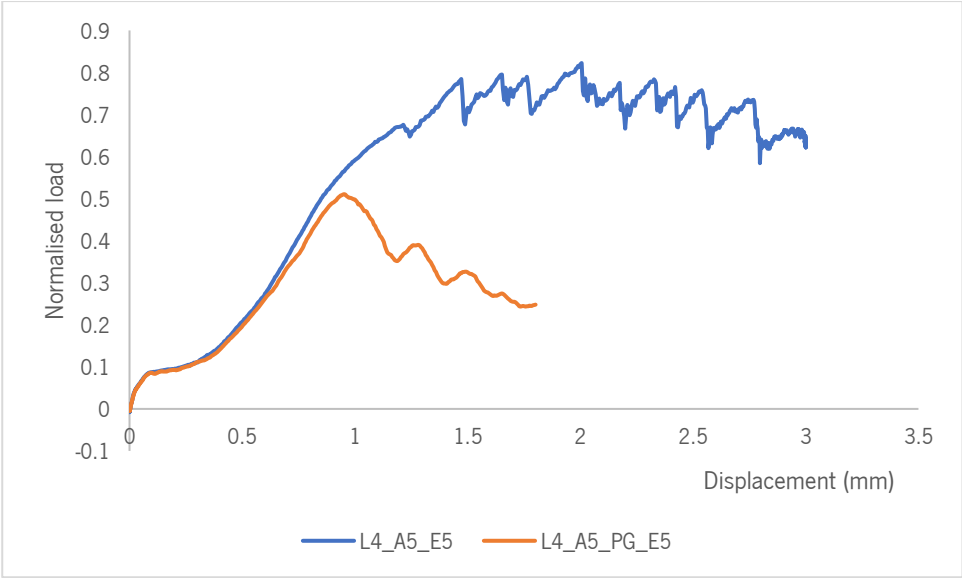

Figure 4.20: Load displacement curve for configuration E5.

It is important to note that in this configuration, the most dominant failure is the bearing failure, as it can be observed in all holes, both for the top and bottom plates. Since the load direction is altered in all the

holes because of the misalignments in the y-direction, the failure seems to be directed at an angle in all holes, see Figure 4.21. In this configuration, both plates seem to have been damaged to the same extent.

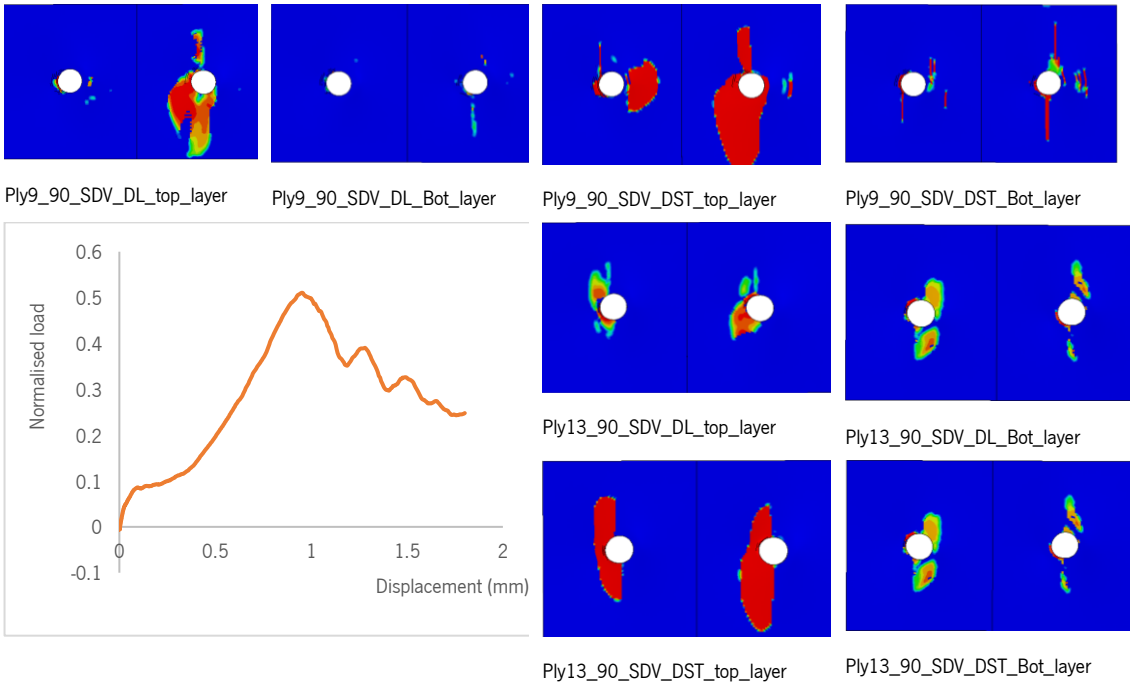

Figure 4.21: E5 configuration, ply 9 and 13 damage plots at the first load drop.

Specimen configuration F5

In this configuration the misalignments are in the x direction in both holes as seen in Detail B and Detail C in Figure 4.22. In detail B there is a 0.5 mm misalignment, while it is -0.5 mm for detail C, both in the x-direction.

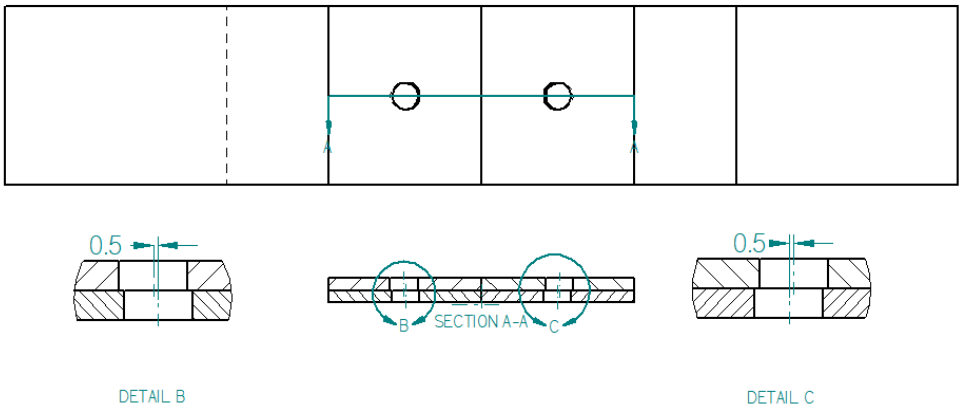

Figure 4.22: Misalignment details for both bolts in the X-direction for configuration F5.

In this type of configuration, one bolt bears load before the other, as shown in Figure 4.23. At a displacement of 1.10 mm, only the right hole bearing surfaces in both the top and bottom plates carry the

load due to the joint's misalignment. As the bearing damage in that area progresses, it creates a plateau until the left holes' bearing surfaces of both plates also begin to carry the load. In this type of joint configuration, premature failure can occur on one side due to uneven load distribution across the assembly, which can have significant implications for structural integrity and safety. Again, the 2 modelling approaches agree well until the first damage onset. In this case, the simulation with 3 elements per ply stopped prematurely due to excessive distortion in the right bearing holes.

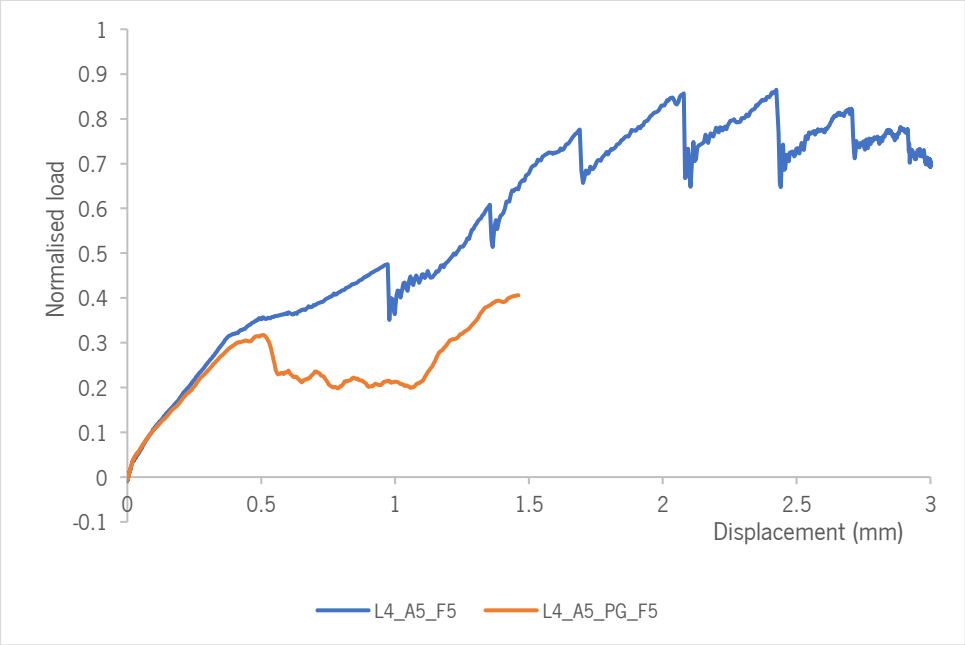

Figure 4.23: load displacement curves for configuration F5.

Both the top and bottom plate damage plots show that the bearing surfaces in the left bolt do not bear any load until approximately 1.07 mm of displacement. This is evident in Figure 4.24, where only the right bearing surfaces are damaged, indicating an unequal stress distribution in the assembly.

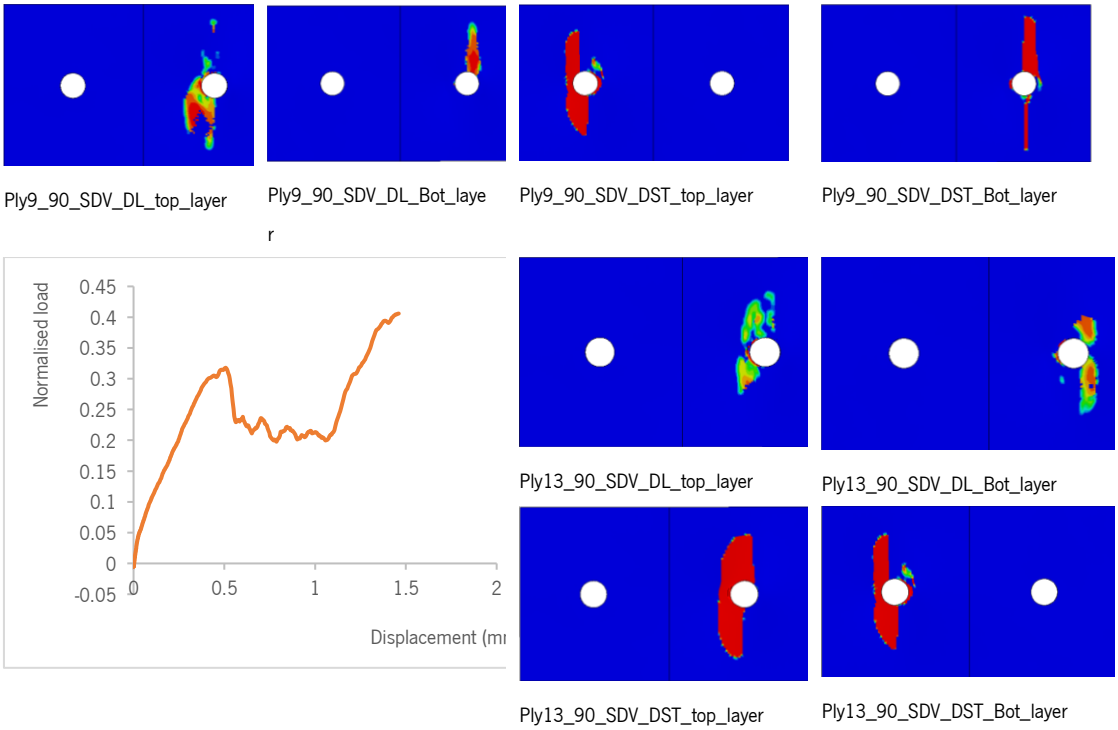

Figure 4.24: F5 configuration, ply 9 and 13 damage plots at first load drop.

4.2.3. Effects of clearances and misalignments on quantities of interest

In this study, an investigation of the effect of hole misalignment and hole clearance effect was carried out on three Quantities of Interest (QoI), namely, stiffness of the joint when the bolt start to transmit in the linear elasic region, first knee point (i.e., when damage starts to develop), and first load drop. This was performed on the macro-scale model (one element through the thickness).

Taking the configuration A0 as the reference for the three quantities of interest, the results in Table 4.4 show the effect of assembly tolerances. In configurations A3 and A5 with the presence of clearances, there is a moderate loss of stiffness, but a more significant drop in the first knee point load, which shows that the clearances affect the damage onset in the joint more than its stiffness.

In configurations B5, C5, and F5, a higher performance reduction is observed with the structure losing above 46% of its stiffness and a decrease in the first knee point load of around 58-61% which implies that these cases of misalignment critically compromise the stiffness and the damage onset load of the joint. Configuration F5, shows a more critical decline in the first load drop as well (52.02%), suggesting a low bearing capacity is a high-risk case scenario in operation. D5 and E5 show an intermediate reduction in

the quantities of interest. Overall, the results indicate that the first knee point load (damage onset load) is more sensitive to both misalignments and clearances and maintaining a better joint/structure performance, it is imperative to have configurations close to the ideal A0.

Table 4.4: Effects of assembly tolerances on joint performance for different quantities of interest.

	Quantity of interest and respective percentage reduction					
Configuration	**Joint stiffness [N/mm]**	**% joint stiffness**	**First knee point load [N]**	**% first knee point load**	**First load drop [N]**	**% in first load drop**
A0	40306.29	0.00	22085.67	0.00	26677.15	0.00
A3	36031.88	-10.60	17582.11	-20.39	25041.06	-6.13
A5	33507.27	-16.87	15611.51	-29.31	23150.46	-13.22
B5	14075.66	-65.08	9058.12	-58.99	19744.70	-25.99
C5	21602.88	-46.40	8691.64	-60.65	19775.13	-25.87
D5	29213.94	-27.52	15919.13	-27.92	23215.20	-12.98
E5	23500.85	-41.69	15000.00	-32.08	21143.57	-20.74
F5	19899.15	-50.63	8605.97	-61.03	12798.82	-52.02

4.3. Uncertainties Quantification (DoE)

For this study, the primary source of uncertainties focused on the misalignments of the holes between the top and bottom plates, with their respective bolt-hole clearance allowed. A non-deterministic approach was used to generate 30 random samples, using a Python script with the condition of minimum clearance to be satisfied, as can be seen in Figure 3.6. Basically, the 4 misalignment values (alfa_1, alfa_2, beta_1, beta_2) were first randomly generated. Then, the minimum clearance needed to the bolt to go through all the hole without penetration was calculated. After this, a random clearance was created in the range between the minimum necessary and 0.5 mm.

The DoE generated with the corresponding clearance value and misalignments are presented in Table 4.5. The parametric Python script was used for generating a model for each of the corresponding 30 samples. During the post-processing, the three quantities of interest described in Section 4.2.3 were used. As can be seen from Table 4.5, the model based on Hashin's criteria is computationally efficient, and, since the

modelling predictions up to the damage onset was the same for both modelling strategies, the uncertainties were propagated using that approach.

Table 4.5: Random samples with uncertainties (misalignments and clearances).

Sample	Alfa_1 [mm]	Alfa_2 [mm]	Beta_1 [mm]	Beta_2 [mm]	Min_clearance [mm]	Hole_clearance [mm]
1	0.124	0.088	-0.113	0.047	0.167	0.393
2	-0.291	-0.130	0.295	0.148	0.414	0.431
3	0.158	0.063	-0.411	-0.219	0.440	0.452
4	0.294	-0.204	0.087	0.196	0.306	0.475
5	-0.216	0.017	-0.098	-0.265	0.266	0.497
6	0.391	0.438	0.176	-0.039	0.440	0.440
7	0.124	0.477	0.235	0.038	0.479	0.483
8	0.260	-0.060	-0.059	0.267	0.273	0.298
9	-0.166	-0.054	-0.061	-0.379	0.383	0.446
10	-0.052	-0.168	0.002	-0.145	0.221	0.468
11	0.306	0.422	-0.185	0.149	0.448	0.463
12	0.074	0.285	-0.373	-0.406	0.496	0.498
13	-0.263	-0.441	0.271	0.182	0.478	0.494
14	0.198	-0.083	-0.173	0.029	0.263	0.448
15	0.245	0.114	-0.272	0.375	0.392	0.497
16	0.442	0.168	0.184	0.118	0.479	0.488
17	0.227	0.265	-0.009	0.362	0.449	0.482
18	-0.299	0.041	-0.126	-0.259	0.324	0.454
19	0.057	0.271	0.203	0.356	0.448	0.484
20	0.400	-0.185	0.063	-0.403	0.444	0.456
21	0.194	0.328	-0.394	-0.359	0.486	0.489
22	0.089	-0.470	0.131	0.038	0.471	0.482
23	-0.103	-0.142	0.472	-0.321	0.483	0.485
24	0.399	0.129	-0.039	0.477	0.495	0.498
25	0.273	0.139	0.156	0.004	0.315	0.330
26	-0.410	0.295	-0.173	0.245	0.446	0.454
27	0.129	0.231	-0.034	-0.004	0.231	0.436

28	-0.481	-0.043	0.079	0.002	0.488	0.493
29	-0.295	-0.351	-0.140	0.123	0.372	0.382
30	-0.007	-0.269	0.211	0.120	0.294	0.464

4.4. Uncertainty Quantification and Management (UQ&M)

Post uncertainty propagation, the simulations were run, and the three quantities of interest (stiffness of the joint, load at the first knee point and the first load drop) were post-processed based for the 30 randomly generated samples. For each of the quantities of interest, the best statistical distribution fitting the data was established and after, the B-value was computed using a function for B-value determination by the CMH17 approach (Python code developed by Joan Ninyerola and Oriol Vallmajó). The B-values were estimated to be within the 95% lower confidence bound on the tenth percentile of 30 samples, depending on the quantity of interest.

Taking the stiffness of the joint as the quantity of interest, the data followed a Weibull cumulative distribution function with two parameters, see Figure 4.25. The B-value obtained was 15567.15 N/mm, and the two parameters being β =5.6863 (known as shape parameter which shows the curve's slope), and α = 27185.1190 (known as the scale parameter, it is the mean of the distribution and the average stiffness past which the joint stops having a linear elastic response).

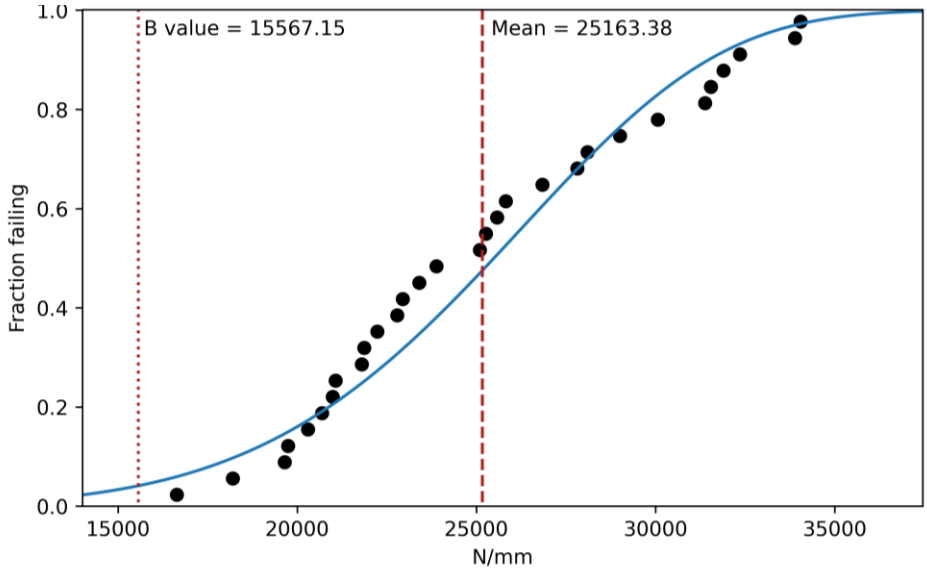

Figure 4.25:Weibull cumulative distribution function curve for n=30 for the stiffness of the joint data B-value.

Second quantity of interest is the first knee point which is quite interesting because it shows what is happening to the joint due to the misalignments and how different misalignments affect the load up taken by the joint. The data set in from this quantity of interest followed a non-parametric cumulative distribution, see Figure 4.26. This caused the data to be scattered on two different sides because of the misalignments. This is explained by different joint misalignment combination values that were introduced as follows. For the configurations in which the misalignment caused the load to be taken by one bolt at first, the first knee

point was observed at a much lower load, However, for cases where the misalignments caused the load to be taken by the two bolts the first knee point occurred at a much higher load. As a result, the B-value obtained for this distribution was 8674.50 N as it had to satisfy the condition of 95% lower confidence bound.

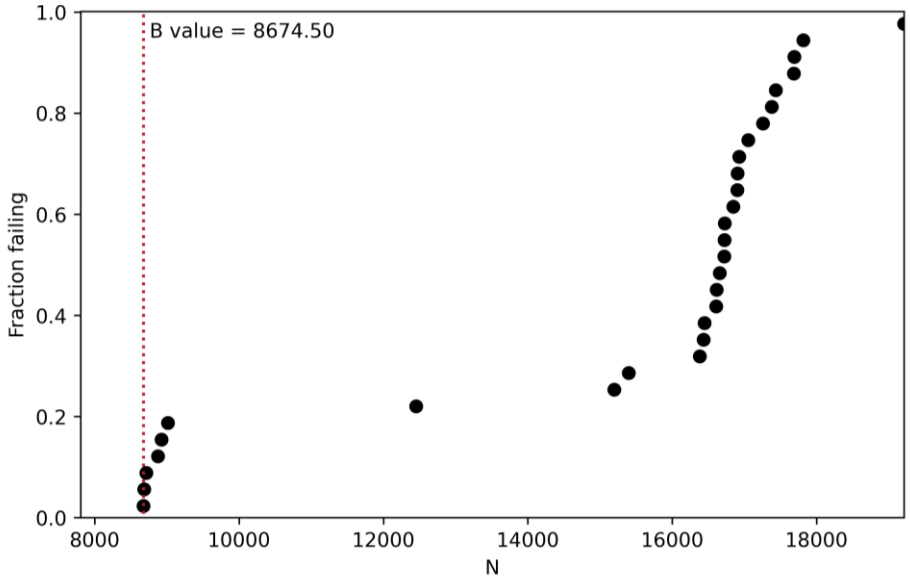

Figure 4.26: Non-parametric cumulative distribution function curve for n-30 for the first knee point load data B-value.

The last quantity of interest investigated was the first load drop in the samples, which is past the non-linear response on the load displacement curve. The population follows a Weibull cumulative distribution function with two parameters, see Figure 4.27, $\beta = 16.2317$ and $\alpha = 22826.4397$. The B-value obtained was 18776.67 N. With most of the data falling close or above the average, this parameter would provide a more reliable design, but needs more testing.

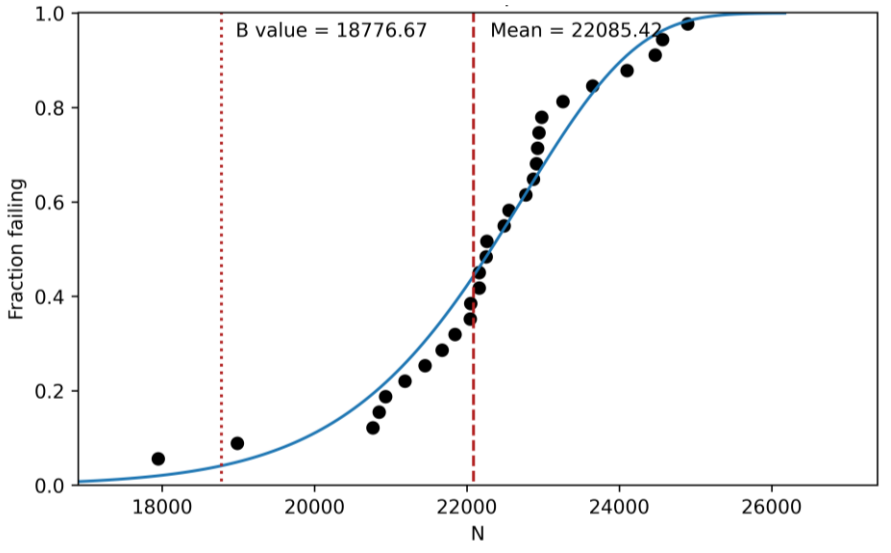

Figure 4.27: Weibull cumulative distribution curve for n=30 for the first load drop data B-value.

4.5. Computation of knock down factors due to the uncertainties

As stated in the literature, a knock down factor is a value indicating by how much the strength of a structure is reduced, ranging from 0-1, where 1 would indicate no reduction. It is computed using the statistical B-value with respect to a reference value. Taking the B-values computed in Section 4.3 and Eq. (3.1), the knock down factor on the assembly for the selected quantities of interest can be computed. The reference value is obtained from the nominal value of the quantity of interest obtained from a configuration without clearances and misalignments, which in this study corresponds to the results obtained from nominal configuration labelled as A0.

4.6. Results and discussion

Although uncertainties such as bolt-hole clearances and hole misalignments influence the overall performance of the structure, each quantity of interest exhibited different value of knock down factors as can be seen in Table 4.6.

Table 4.6: Knock down factors for the three quantities of interest (QoI).

QoI	Nominal value (A0)	B-Value	KDF
Stiffness of the joint [N/mm]	40306.29	15567.15	0.39
First knee point load [N]	22085.67	8674.50	0.39
First load drop [N]	26677.15	18776.67	0.70

4.7. Discussion on Knock down factors obtained

The stiffness of the joint offers a conservative value of knock down factor, this is due to the overall behaviour of the joint with uncertainties and the effect they have on the overall performance of the structure. Since the uncertainties were propagated in a non-deterministic manner, and the increase in clearance or misalignments drastically affected the stiffness, this justifies the value of the knock down factor obtained.

Similarly with the first knee point, which was extremely dependent on the misalignment and clearance values. In some cases, the misalignments caused uneven loading in the bolts between bolt one and bolt two, where a single bolt took the load in the first instants of loading; hence having a lower load value at the first knee point which gives a conservative B-value.

A much larger KDF can be seen when the quantity of interest is the first load drop. This can be attributed to the reason being that most of those values were the ultimate load bearing capacities. In the literature it is shown that clearances do not affect much the value of ultimate load bearing capacity. The misalignment by itself was seen earlier in this work that could have some important effect, but not as much as in the other QoI. Hence, the KDF obtained is much higher.

The results from this work offer a good overview of the complex design of bolted joints, where it can clearly be seen that designing them using nominal values is not accurate. Uncertainty propagation is mandatory to account for extreme cases which could occur in reality. As a next step, experimental data shall be obtained for comparing the KDF obtained here with experiments, and also to clarify which of the modelling strategies is the best one.

5. CHAPTER 5: CONCLUSIONS AND FUTURE WORK

This study aimed to model the effect of assembly tolerances on the structural performance of multi-bolted joints by propagating uncertainties. Three quantities of interest were explored: the initial stiffness, the first knee point and the first load drop. The findings show that, depending on the quantity of interest selected, a different value of knock down factor was obtained. Especially, the KDF was quite low (0.39) for the initial stiffness and the first knee point, while it was much larger (0.7) for the first load drop. According to the observations, the findings also agree with the existing literature, which states that the ultimate bearing capacity of a joint is not affected by the clearances, and in case of multi bolts with misalignments the load is not distributed equally between the bolts but evens as at higher loads [12]. From the findings of this study, engineers can design fail-safe joints through a better understanding of the effects of misalignments and clearances in multi-bolt joints used in different structural applications.

The findings in this study are limited to a joint made of a quasi-isotropic laminate, with a constant bolt preload, so they cannot be generalized for different configurations of ply stacking, such as soft and hard laminates, cases accounting for material uncertainty or loading uncertainty (such as different preload values, misalignment in the applied loads, etc.). However, this study lays a foundation for developing a framework to determine knock down factors caused by clearance and hole misalignment uncertainties present in the structure.

During the development of this study, it was noted that bolt preload and ply stacking sequences, along with laminate thickness, also affect the structure's performance. Therefore, it is recommended for future studies to combine these source of uncertainties with clearances and misalignments while determining the knock down factors on structure considering the assembly tolerances. Results should also be validated with experimental data.

6. REFERENCES

[1] F. Abdi, E. Clarkson, C. Godines, S. DorMohammadi, and A. De Fenza, "A-B basis allowable test reduction approach and composite generic basis strength values," in *18th AIAA Non-Deterministic Approaches Conference*, American Institute of Aeronautics and Astronautics Inc, AIAA, 2016. doi: 10.2514/6.2016-0951.

[2] "DEPARTMENT OF DEFENSE HANDBOOK COMPOSITE MATERIALS HANDBOOK VOLUME 1. POLYMER MATRIX COMPOSITES GUIDELINES FOR CHARACTERIZATION OF STRUCTURAL MATERIALS AMSC N/A AREA CMPS DISTRIBUTION STATEMENT A. Approved for public release; distribution unlimited," 2002.

[3] S. D. Thoppul, J. Finegan, and R. F. Gibson, "Mechanics of mechanically fastened joints in polymer-matrix composite structures - A review," Mar. 2009. doi: 10.1016/j.compscitech.2008.09.037.

[4] S. Li, S. Zhang, H. Li, X. Qin, X. Wu, and L. Gui, "Numerical and experimental investigation of fitting tolerance effects on bearing strength of CFRP/Al single-lap blind riveted joints," Feb. 01, 2022, *Elsevier Ltd*. doi: 10.1016/j.compstruct.2021.115022.

[5] S. Norisam and A. B. Abdullah, "Quality and performance assessments of drilling and punching in the hole-making process of a composite panel: A comparative study," *Hole-Making and Drilling Technology for Composites*, pp. 211–226, 2019, doi: 10.1016/B978-0-08-102397-6.00015-5.

[6] D. F. Liu, Y. J. Tang, and W. L. Cong, "A review of mechanical drilling for composite laminates," *Compos Struct*, vol. 94, no. 4, pp. 1265–1279, Mar. 2012, doi: 10.1016/J.COMPSTRUCT.2011.11.024.

[7] M. J. Liu, S. Yu, and Q. Y. Zhao, "Study on Fatigue Performance of Composite Bolted Joints with Bolt-Hole Delamination," in *IOP Conference Series: Materials Science and Engineering*, Institute of Physics Publishing, Mar. 2018. doi: 10.1088/1757-899X/326/1/012004.

[8] B. G. Kiral, "Effect of the clearance and interference-fit on failure of the pin-loaded composites," *Mater Des*, vol. 31, no. 1, pp. 85–93, Jan. 2010, doi: 10.1016/J.MATDES.2009.07.009.

[9] C. Bo, Z. Yang, L. Wang, and H. Chen, "A comparison of tolerance analysis models for assembly," *International Journal of Advanced Manufacturing Technology*, vol. 68, no. 1–4, pp. 739–754, Sep. 2013, doi: 10.1007/s00170-013-4795-2.

[10] M. A. Mccarthy, V. P. Lawlor, W. F. Stanley, and C. T. Mccarthy, "Bolt-hole clearance effects and strength criteria in single-bolt, single-lap, composite bolted joints." [Online]. Available: www.elsevier.com/locate/compscitech

[11] G. Kelly and S. Hallström, "Bearing strength of carbon fibre/epoxy laminates: Effects of bolt-hole clearance," *Compos B Eng*, vol. 35, no. 4, pp. 331–343, 2004, doi: 10.1016/j.compositesb.2003.11.001.

[12] V. P. Lawlor, M. A. McCarthy, and W. F. Stanley, "An experimental study of bolt-hole clearance effects in double-lap, multi-bolt composite joints," *Compos Struct*, vol. 71, no. 2, pp. 176–190, Nov. 2005, doi: 10.1016/j.compstruct.2004.09.025.

[13] Y. Cao, Z. Cao, Y. Zuo, L. Huo, J. Qiu, and D. Zuo, "Numerical and experimental investigation of fitting tolerance effects on damage and failure of CFRP/Ti double-lap single-bolt joints," *Aerosp Sci Technol*, vol. 78, pp. 461–470, Jul. 2018, doi: 10.1016/j.ast.2018.04.042.

[14] Y. Zuo, Z. Cao, G. Zheng, and Q. Zhang, "Damage behavior investigation of CFRP/Ti bolted joint during interference fit bolt dynamic installation progress," *Eng Fail Anal*, vol. 111, Apr. 2020, doi: 10.1016/j.engfailanal.2020.104454.

[15] R. Li, R. Xiao, H. Gao, Y. Bao, and X. Liu, "Research Paper Effects of Hole Perpendicularity Error on Load Distribution in Single-Lap Double-Bolt Composite Joints," 2018.

[16] O. Vallmajó, M. Descamps, A. Arteiro, and A. Turon, "Effect of ply misalignment on the notched strength of composite laminates."

[17] C. Schoenholz, E. Zappino, M. Petrolo, and N. Zobeiry, "Efficient analysis of composites manufacturing using multi-fidelity simulation and probabilistic machine learning," *Compos B Eng*, vol. 280, Jul. 2024, doi: 10.1016/j.compositesb.2024.111499.

[18] H. Fu and N. Zobeiry, "A Theory-Guided Machine Learning and Reduced-Order Finite Element Modeling Framework to Accelerate Process Simulation of Aerospace Composite Parts," *Proceedings of ASME 2023 Aerospace Structures, Structural Dynamics, and Materials Conference, SSDM 2023*, Oct. 2023, doi: 10.1115/SSDM2023-107132.

[19] A. Eskandariyun *et al.*, "A Novel Machine Learning Framework for Digital Estimation of Allowables in Aerospace Composites," *Proceedings of ASME 2024 Aerospace Structures, Structural Dynamics, and Materials Conference, SSDM 2024*, Jun. 2024, doi: 10.1115/SSDM2024-121597.

[20] G. Kolks and K. I. Tserpes, "Efficient progressive damage modeling of hybrid composite/titanium bolted joints," *Compos Part A Appl Sci Manuf*, vol. 56, pp. 51–63, 2014, doi: 10.1016/j.compositesa.2013.09.011.

[21] O. Vallmajó *et al.*, "Virtual calculation of the B-value allowables of notched composite laminates," *Compos Struct*, vol. 212, pp. 11–21, Mar. 2019, doi: 10.1016/j.compstruct.2018.12.049.

[22] G. Abumeri, F. Abdi, K. S. Raju, J. Housner, R. Bohner, and A. McCloskey, "Cost Effective Computational Approach for Generation of Polymeric Composite Material Allowables for Reduced Testing," in *Advances in Composite Materials - Ecodesign and Analysis*, InTech, 2011. doi: 10.5772/14528.

[23] J. Ninyerola Gavaldà, I. R. Cózar, J. M. Guerrero, S. Abdel-Monsef, A. Sasikumar, and A. Turon, "A validated simulation methodology for determining single lap shear allowable strength in thermoplastic polymer composites," *Compos B Eng*, vol. 289, Jan. 2025, doi: 10.1016/j.compositesb.2024.111909.

[24] R. Van Wagenen, "A Guide to Structural Factors for Advanced Composites Used on Spacecraft," 1989.

[25] I. R. Cózar, F. Otero, P. Maimí, E. V. González, A. Turon, and P. P. Camanho, "An enhanced constitutive model to predict plastic deformation and multiple failure mechanisms in fibre-reinforced polymer composite materials," *Compos Struct*, vol. 330, Feb. 2024, doi: 10.1016/j.compstruct.2023.117696.

[26] I. R. Cózar *et al.*, "Influence of unidirectional composite failure envelope shape on predicting compressive failure of a laminate with a filled-hole," *Compos B Eng*, vol. 276, May 2024, doi: 10.1016/j.compositesb.2024.111352.